Supplement of Biogeosciences, 23, 2761–2785, 2026
https://doi.org/10.5194/bg-23-2761-2026-supplement

Biogeosciences Open Access EGU

Supplement of

Spatial heterogeneity of soil organic matter and microbial community composition across ice-wedge polygons and soil layers in Arctic lowland tundra

Victoria Martin et al.

Correspondence to: Victoria Martin (victoria.sophie.martin@univie.ac.at)

Supplementary

Table of Contents

S1. Study area and soil sampling 3

Supplementary Tables

[Table S1]

(a) Polygon types, coordinates, and vegetation composition in sampled soil pits

(b) Active layer depths and in-situ soil temperatures

(c) Summary of sample layout 4-6

Supplementary Figures

[Fig. S1] Examples for investigated (a) polygon types; (b) soil layers 7

S2. Physicochemical soil parameters and stoichiometry 9

Supplementary Tables

[Table S2] Physicochemical soil parameters and stoichiometry across (a) polygon types; (b) soil layers 10-12

S3. Chemical composition of soil organic matter 13

Supplementary Tables

[Table S3] Correlations between SOM compound group abundances and soil C content 15

Supplementary Figures

[Fig. S2] Number of shared and unique pyrolysis products across (a) polygon types; (b) soil layers 16

[Fig. S3] Abundances of SOM compound groups across (a) polygon types; (b) soil layers 17

[Fig. S4] Relative abundances of SOM compound groups across (a) polygon types; (b) soil layers

..... 18

S4. Soil microbial communities 19

Supplementary Tables

[Table S4] Cycling conditions used for digital droplet PCR (ddPCR) 21

S4.1. Bacterial and archaeal communities 23

Supplementary Tables

[Table S5] Interactive effects of polygon type and soil layer category on bacterial and archaeal community composition (corresponding to Fig. 3 in main text) 23

[Table S6] ddPCR-informed abundance estimates of selected bacterial and archaeal phyla 24-29

Supplementary Figures

[Fig. S5] Bacterial and archaeal richness, diversity, and abundance estimates 30

[Fig. S6] Number of shared and unique bacterial and archaeal ASVs across (a) polygon types; (b) soil layers 32

[Fig. S7] Archaeal abundance (a) ddPCR-informed abundance; (b) relative abundance 33

[Fig. S8] Heatmap: ddPCR-informed abundance estimates of bacterial and archaeal phyla 34

S4.2. Fungal communities 35

Supplementary Tables

[Table S7] ddPCR-informed abundance estimates of fungal phyla 35-37

Supplementary Figures

[Fig. S9] Fungal richness, diversity, and abundance estimates 38

[Fig. S10] Number of shared and unique fungal ASVs across (a) polygon types; (b) soil layers 40

[Fig. S11] Heatmap: ddPCR-informed abundance estimates of fungal phyla 41

S5. Extracellular enzymatic activity potential 42

Supplementary Tables

[Table S8] Correlations between enzyme activities and Soil C, N, P contents 42

[Table S9] Interactive effects of polygon type and soil layer category on potential extracellular enzymatic activities (corresponding to Fig. 5 in main text) 43-44

Supplementary Figures

[Fig. S12] Potential extracellular enzymatic activities per gram dry soil 43

S6. Statistics 47

S7. References 49

S1. Study area and soil sampling

We studied two areas classified as Arctic lowland ice-wedge polygon tundra, located on the coastal plain of the Yukon, Western Canada (Figure 1). The first focus area comprised two small lagoons called Ptarmigan Bay (69°27'N, 139°05'W) and Whale Bay (69°25'N, 138°59'W). The second focus area, approximately 40 km further towards the west, called Komakuk Beach (69°35'N, 140°10'W), is a small coastal catchment positioned between two alluvial fans. Despite their close vicinity, the areas differ in their glaciation history. Throughout the Pleistocene, the areas of Ptarmigan Bay and Whale Bay were covered by ice sheets, whereas the Komakuk Beach further west stayed unglaciated (Dyke and Prest, 1987; Fritz et al., 2012). The surface geology mainly comprises lacustrine, fluvial (Ptarmigan Bay and Komakuk Beach) and morainal deposits (Whale Bay) (Fritz et al., 2012; Rampton, 1982).

The periglacial landscape is characterized by a mosaic of ice-wedge polygon networks, mires, beaded streams, and thermokarst lakes (Rampton, 1982; Speetjens et al., 2022), underlain by continuous permafrost with a high ground ice content (Couture and Pollard, 2017; Westerveld et al., 2023). The climate is classified as Polar Tundra (Beck et al., 2018). Recorded mean annual temperatures (1972 - 2000) at the climate stations Komakuk Beach and Shingle Point (68° 57'N, 137° 13'W) were - 11 °C (± 2.0 °C) and - 9.9 °C (± 4.5 °C). Average summer temperatures (June-August) were 6 °C (± 1.6 °C) and 8.6 °C (± 1.6 °C). Mean annual precipitation (1972 – 2000) was 161 mm and 254 mm correspondingly (Canadian Climate Normals & Averages). The vegetation period lasts approximately from June to September (Frank-Fahle et al., 2014). The vegetation map defines the area as bioclimatic subzone E/ low Arctic shrub tundra (Walker et al., 2005).

Differences in microtopography and relief are strong determinants for the identity of the prevailing soil suborder and plant species composition. Turbic Cryosols were present in the drier centres of HCPs and FCPs (Canadian System of Soil Classification, Soil Classification Working Group, 1998). These soils harbor up to 40 cm thick organic horizons with material being of various decomposition stages, followed by a pronounced silt- and clay-rich mineral subsoil layer which commonly exhibits cryoturbations or gleyic features (Tarnocai, 2004). Dwarf-shrubs (e.g., *Betula nana*, *Salix arctica*, *Salix alaxensis*, *Empetrum nigrum*, *Vaccinium sp*.), forbs (e.g., *Rubus chamaemorus, Dryas sp*.) and lichens dominated the centres of HCPs. FCPs were mainly characterised by *Eriophorum vaginatum* tussocks and dwarf-shrubs. Inundated centres of LCP harbored Organic Cryosols, which show a more than 40 cm thick characteristic sequence from fibric to hemic to sapric sphagnum- or sedge- derived material with increasing depth. The dominant plant groups were graminoids (*Carex aquatilis*, *Eriophorum vaginatum, Eriophorum angustifolium*), brown mosses (Amblystegiaceae), and peat mosses (*Sphagnum sp.*) (Brooks and Lane, 2011; Rampton, 1982; Walker et al., 2005). Towards the drier rims, Organic Cryosols transitioned into Cryosols of the Gleysolic or Static type, indicated by higher dwarf shrub abundance.

Table S1 (a). *Sampled soil pits, including polygon type, coordinates, and vegetation composition.*

Soil pit	Study Area	Polygon type	N	W	Comments
1	Ptarmigan Bay	HCP	69° 27.862500'	139° 4.939320'	tussock tundra, *Salix sp*., *Betula sp*., *Sphagnum sp*., mosses, lichens
2	Ptarmigan Bay	HCP	69° 27.860040'	139° 5.103600'	*Salix sp*., *Betula sp*., *Empetrum nigrum*, *Dryas sp*., *Vaccinium sp*., lichens
3	Ptarmigan Bay	HCP	69° 27.881220'	139° 5.219760'	*Salix sp*., *Betula sp*., *Rubus chamaemorus*, *Vaccinium sp*., mosses, lichens
4	Whale Bay	FCP	69° 25.561920'	138° 59.929800'	tussock tundra, *Salix sp*., *Betula sp*., graminoids
5	Whale Bay	FCP	69° 25.601040'	139° 0.145080'	tussock tundra, *Salix sp*., Betula sp., *Vaccinium sp*., *Ledum sp.,* mosses
6	Whale Bay	FCP	69° 25.522920'	138° 59.908980'	tussock tundra, *Salix sp*., *Vaccinium sp*., *Ledum sp.,* mosses
7	Ptarmigan Bay	LCP	69° 27.913140'	139° 5.086560'	Sedge-dominated, *Eriophorum sp.*, *Sphagnum sp*., brown mosses
8	Ptarmigan Bay	LCP	69° 27.922800'	139° 5.084160'	Sedge-dominated, *Eriophorum sp*., *Sphagnum sp*., brown mosses
9	Ptarmigan Bay	LCP	69° 27.917880'	139° 5.030940'	Sedge-dominated, *Eriophorum sp*., *Sphagnum sp*., brown mosses
10	Komakuk Beach	HCP	69° 35.590020'	140° 9.880020'	*Betula sp*., *Dryas sp*., *Rubus chamaemorus*, mosses, lichens
11	Komakuk Beach	HCP	69° 35.577000'	140° 9.826980'	*Betula sp*., *Salix sp*., *Vaccinium sp*., *Rubus chamaemorus*, mosses
12	Komakuk Beach	HCP	69° 35.610000'	140° 9.768000'	tussock tundra, *Betula sp*., *Empetrum nigrum*, mosses, lichens, fungi
13	Komakuk Beach	FCP	69° 35.338020'	140° 9.847020'	flat tundra surrounded by wetlands, *Carex sp*., *Salix sp*.
14	Komakuk Beach	FCP	69° 35.551980'	140° 9.454020'	flat tundra, *Carex sp*., *Eriophorum sp., Betula sp*., *Vaccinium sp*., mosses
15	Komakuk Beach	FCP	69° 35.752020'	140° 9.292980'	flat tundra, *Carex sp*., Salix sp., mosses, *Eriophorum sp*.
16	Komakuk Beach	LCP	69° 34.623000'	140° 10.621980'	Sedge-dominated, *Carex sp*., *Salix sp*., *Sphagnum sp*., brown mosses
17	Komakuk Beach	LCP	69° 34.852020'	140° 11.119020'	Sedge-dominated, *Carex sp.*, *Salix sp*., *Sphagnum sp*., brown mosses
18	Komakuk Beach	LCP	69° 34.894980'	140° 10.929000'	Sedge-dominated, *Eriophorum sp*., brown mosses

Dry areas of high-centered polygons (HCPs) were typically dominated by dwarf shrubs, forbs, and lichens, whereas centers of low-centered polygons (LCPs) were characterized by water-saturated conditions and vegetation dominated by graminoids and peat- and brown mosses..

Table S1 (b). *Sampled soil pits, including active layer depths and in-situ soil temperatures.*

Soil pit	Study Area	Polygon type	AL depth (cm)	In-situ Soil Temp (°C)			
				5 cm	15 cm	25 cm	PF Table
1	Ptarmigan Bay	HCP	35.0	7.7	2.5	1.8	1.4
2	Ptarmigan Bay	HCP	30.0	4.5	2.8	1.7	1.5
3	Ptarmigan Bay	HCP	31.0	4.3	3.9	3.6	0.9
4	Whale Bay	FCP	40.0	4.9	1.9	0.9	0.3
5	Whale Bay	FCP	40.0	4.4	4.0	2.5	1.9
6	Whale Bay	FCP	40.0	7.7	2.9	2.3	1.2
7	Ptarmigan Bay	LCP	40.0	4.8	4.4	3.8	2.0
8	Ptarmigan Bay	LCP	30.0	3.8	3.6	3.4	2.5
9	Ptarmigan Bay	LCP	30.0	6.6	5.6	4.5	n.a.
10	Komakuk Beach	HCP	30.0	5.1	3.4	2.4	1.6
11	Komakuk Beach	HCP	22.5	3.6	2.5	-	1.5
12	Komakuk Beach	HCP	30.5	5.5	4.5	3.6	2.3
13	Komakuk Beach	FCP	28.0	7.4	2.5	1.4	0.4
14	Komakuk Beach	FCP	30.0	4.7	4.3	3.4	2.6
15	Komakuk Beach	FCP	22.5	4.6	1.1	-	0.1
16	Komakuk Beach	LCP	45.0	6.6	6.2	4.7	0.8
17	Komakuk Beach	LCP	52.0	6.8	5.6	3.6	n.a.
18	Komakuk Beach	LCP	40.0	5.7	4.3	3.0	0.2

Average active layer depths ranged between 30 ± 2 cm (mean ± SE) in high-centered (HCPs), 33 ± 3 cm in flat-centered (FCPs), and 40 ± 4 cm in low-centered (LCPs) polygons. Average in-situ soil temperatures declined from 5.5 ± 0.3 °C (mean ± stderr) at the surface (5 cm depth), to 3.7 ± 0.3 °C at 15 cm depth, to 2.9 ± 0.3 °C in 25 cm depth and to 1.3 ± 0.2 °C at the permafrost table.

Table S1 (c). *Summary of sample layout.*

Ptarmigan Bay & Whale Bay (n=39)				Komakuk Beach (n=42)			
	LCP (n=8)	FCP (n=17)	HCP (n=14)		LCP (n=12)	FCP (n=15)	HCP (n=15)
organic (n=15)	n=4	n=6	n=5	organic (n=20)	n=8	n=6	n=6
mineral (n=7)	n=1	n=3	n=3	mineral (n=7)	n=1	n=3	n=3
cryoturbated (n=7)	n=0	n=4	n=3	cryoturbated (n=6)	n=0	n=3	n=3
permafrost (n=10)	n=3	n=4	n=3	permafrost (n=9)	n=3	n=3	n=3

A total of 81 soil samples were collected and categorized by polygon type (LCP: n = 20, FCP: n = 32, HCP: n =29), and by soil layer (organic topsoil: n = 35, mineral subsoil: n = 14, cryoturbated material: n = 13, and upper permafrost: n = 19). Due to natural field heterogeneity and soil-pit specific differences in soil horizon development, an imbalanced sampling design emerged (organic: LCP = 12, FCP = 12, HCP = 11; mineral: LCP = 2, FCP = 6, HCP = 6; cryoturbated: LCP = 0, FCP = 7, HCP = 6; permafrost: LCP = 6, FCP = 7, HCP = 6). Abbreviations: HCPs = high-centered-, FCPs = flat-centered-, LCPs = low-centered polygons.

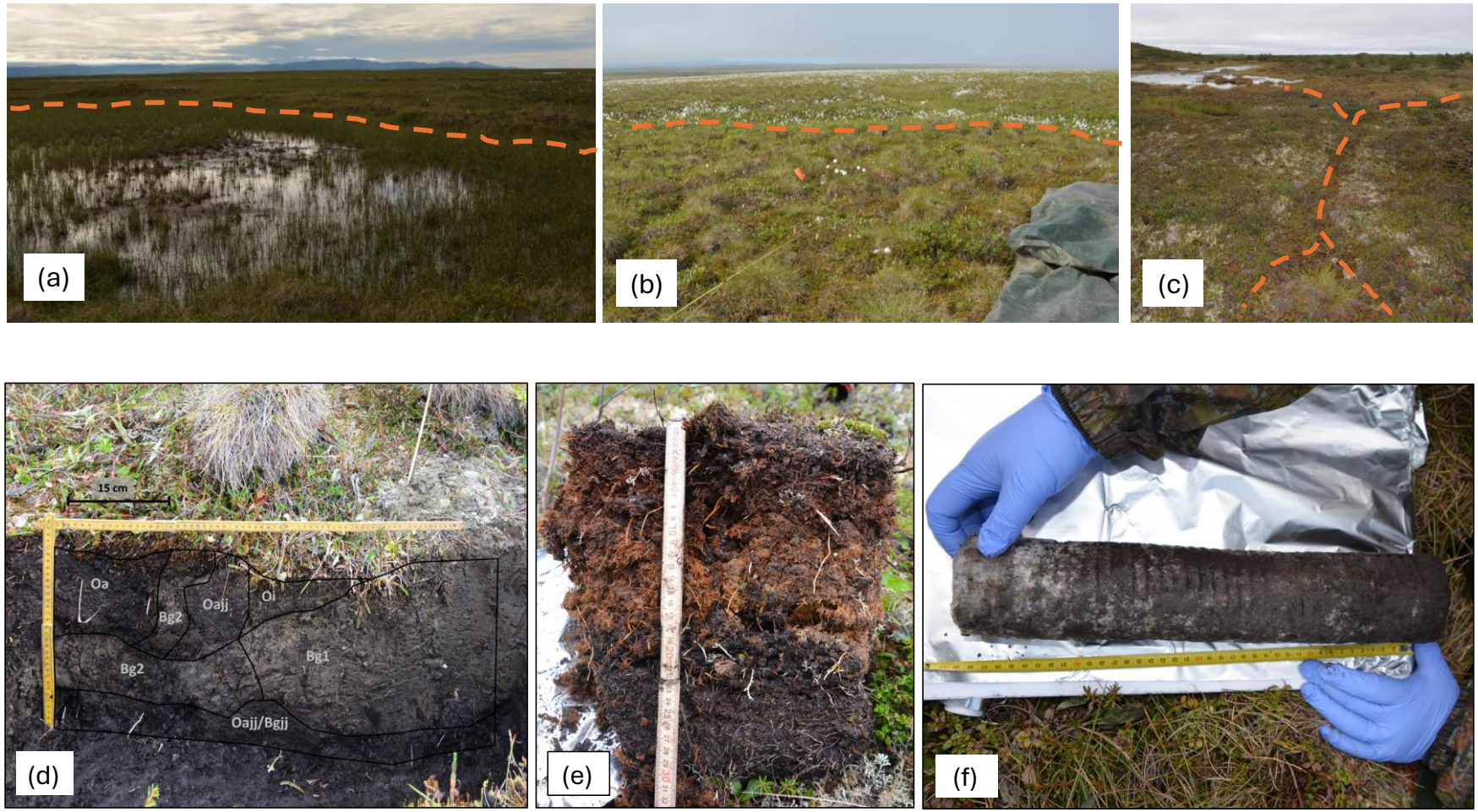

Figure S1. *Examples for investigated ice-wedge polygon types and soil layers. Orange dotted lines roughly mark polygon borders.*

(a) *Low-centered polygon (LCP), with a dry, elevated rim around inundated center.* ***(b)*** *Flat-centered polygon (FCP) with the presence of cotton grass indicating wetter troughs around the flat-center.* ***(c)*** *High-centered polygon (HCP), with mosses indicating wetter troughs surrounding a drier, elevated center.* ***(d)*** *Active layer sampling from soil pits (applied to HCPs and FCPs); horizon boundaries (perspective corrected) were drawn on the image:(source:* Wagner et al., (2023). ***(e)*** *Active layer sampling from LCPs (extracted peat block).* ***(f)*** *Frozen permafrost sampling (example of a core extracted using a gas powered SIPRE corer. Note that 'permafrost layer' in this manuscript refers to the upper 10 cm). Photo credits: Julia Wagner and Victoria Martin.*

S2. Physicochemical soil parameters and stoichiometry

In the field, samples were weighed for bulk density measurements (see Wagner et al., 2023). Gravimetric soil water content (g H_2O g^{-1} DW) was determined at the facilities of the Aurora Research Institute, Inuvik, Canada, before transporting the samples to Vienna (80 °C for 48 hours). Soil pH was determined in a 1:5 (w/v) soil:MQ water slurry using a Sentron SI600. Aliquots of dry soils were ground to fine powder using a ball-mill (MM-2000, Retsch, Germany). Subsequently, 1-8 mg per sample (depending on the anticipated differences in C content between soil layer categories) were weighed into tin capsules and analyzed for total carbon (mg C g^{-1} DW) and nitrogen (mg N g^{-1} DW) contents via elemental analyzer (EA 1110, CE Instruments, Italy) coupled to a continuous-flow isotopic ratio mass spectrometer (IRMS, DeltaPlus, Finnigan MAT). The soils did not contain any carbonates, which was tested by adding 1M HCl to the samples before subjecting them to the EA-IRMS. Isotopic signatures ($\delta^{13}C$, $\delta^{15}N$, ‰) were expressed relative to the international standard VPDB. Soil C:N, C:P, and N:P ratios were calculated on a mass basis. Pools of dissolved C and N (DOC, TDN; mg g^{-1} DW) were determined with a TOC/TN-Analyzer (Shimadzu TOC-VCP/CPNTNM-1, Shimadzu, Korneuburg, Austria) in 1M KCl extracts (soil to solution ratio 1:7.5 (w/v)). The soil total phosphorus pool (Soil P) was obtained via a modified ignition method by (Kuo, 1996), which mediates the conversion of organic bound P to inorganic P. Therefore, 200 - 500 mg dry and milled soils were combusted for 5 h at 450 °C, (muffle device Heraeus M1100/1) and then extracted for 16 hours with 10 ml 0.5M H_2SO_4. Soil total Phosphorus concentrations (mg P g^{-1} DW) were measured in the fresh extracts following the photometric malachite-green assay after (D'Angelo and Crutchfield, 2001) All above mentioned extracts have been filtered using Whatman™ quantitative ashless cellulose filter paper, grade 40.

The data is accessible under 10.5281/zenodo.18631833.

Table S2 (a). *Physicochemical soil parameters and stoichiometry across ice-wedge polygon types.*

	LCP	FCP	HCP	Polygon Type Effect
Bulk Density (g DW cm^{-3})	0.31 ± 0.05 (a) [n=19]	0.64 ± 0.10 (a) [n=30]	0.55 ± 0.08 (a) [n=26]	p = 0.231 (Chi^2 = 2.93)
pH (MQ)	5.72 ± 0.09 (b)	5.92 ± 0.05 (a)	5.66 ± 0.06 (b)	**p = 0.004** (Chi^2 = 10.92)
SWC (g g^{-1} DW)	2.93 ± 0.33 (a)	2.20 ± 0.32 (a)	2.03 ± 0.27 (a)	p = 0.603 (F = 0.51)
δ^{13}C (‰)	-27.90 ± 0.13 (a)	-26.73 ± 0.12 (b)	-27.42 ± 0.18 (a)	**p < 0.0001** (Chi^2 = 22.1)
δ^{15}N (‰)	0.34 ± 0.13 (b)	1.31 ± 0.20 (a)	1.63 ± 0.22 (a)	**p = 0.002** (F = 9.77)
Soil C (mg g^{-1} DW)	312.37 ± 30.81 (a)	204.19 ± 21.68 (a)	229.65 ± 23.34 (a)	**p = 0.059** (F = 3.31)
Soil N (mg g^{-1} DW)	18.1 ± 1.90 (a)	10.04 ± 0.91 (b)	12.14 ± 1.21 (b)	**p = 0.003** (Chi^2 = 11.72)
Soil P (mg g^{-1} DW)	0.43 ± 0.03 (*int)	0.68 ± 0.05 (*int) [n=30]	0.63 ± 0.06 (*int)	**p = 0.007** (F = 5.34)
Soil C:N	17.54 ± 0.37 (a)	20.09 ± 1.57 (a)	19.42 ± 0.98 (a)	p = 0.375 (Chi^2 = 3.11)
Soil C:P	783.09 ± 91.44 (a)	305.98 ± 31.02 (b) [n=30]	389.45 ± 37.03 (b)	**p < 0.0001** (F = 22.07)
Soil N:P	45.06 ± 5.30 (a)	15.49 ± 1.04 (b) [n=30]	20.05 ± 1.70 (b)	**p < 0.0001** (F = 37.7)
DOC (µg g^{-1} DW)	551.99 ± 76.89 (a)	355.06 ± 64.63 (a)	400.95 ± 87.34 (a)	p = 0.076 (Chi^2 = 5.15)
TDN (µg g^{-1} DW)	38.51 ± 6.07 (a)	26.63 ± 7.57 (a)	30.89 ± 6.14 (a)	p = 0.404 (F = 0.95)
DOC:TDN	17.69 ± 2.66 (a)	20.49 ± 3.21 (a)	16.01 ± 2.32 (a)	p = 0.122 (F = 2.17)

*Presented are means ± SE (LCP: n = 20, FPT: n = 32, HCP: n = 29; with deviations noted in the table). Statistical results from linear mixed-effects models (Type II ANOVA; p-values and F-statistics) are shown in the right column. When model assumptions were not met, Kruskal Wallis tests were applied (p-values and Chi² statistics). Pairwise comparisons (Tukey-adjusted estimated marginal means or Bonferroni-adjusted pairwise Wilcoxon tests) are indicated by letter groupings in brackets. Significant interactions between polygon type and soil layer are marked with (*int).* ***Interactive effects:*** *Soil P (mg g-1 DW) was significantly lower in the organic layer of LCPs compared to FCPs and HCPs (LME: p = 0.049, F = 2.4; pairwise comparisons for the organic layer: LCP vs. FCP p = 0.0001, t = -4.5;*

LCP vs. HCP $p < 0.0001$, $t = -4.8$). Abbreviations: SWC = soil water content, DOC = dissolved organic carbon, TDN = total dissolved nitrogen; HCPs = high-centered-, FCPs = flat-centered-, LCPs = low-centered polygons.

Table S2 (b). *Physicochemical soil parameters and stoichiometry across soil layers.*

	organic	mineral	cryoturbated	permafrost	Soil Layer Effect
Bulk Density (g DW cm^{-3})	0.20 ± 0.02 (c)	1.27 ± 0.08 (a) [n=13]	0.64 ± 0.10 (b) [n=8]	0.56 ± 0.09 (b)	**p < 0.0001** (Chi^2 = 49.02)
pH (MQ)	5.63 ± 0.06 (b)	5.91 ± 0.06 (ab)	5.80 ± 0.09 (ab)	5.94 ± 0.06 (a)	**p = 0.009** (Chi^2 = 11.51)
SWC (g g^{-1} DW)	3.72 ± 0.23 (a)	0.45 ± 0.03 (c)	1.41 ± 0.19 (b)	1.75 ± 0.18 (b)	**p < 0.0001** (F = 80.21)
δ^{13}C (‰)	-27.34 ± 0.15 (a)	-27.59 ± 0.26 (a)	-27.16 ± 0.23 (a)	-26.96 ± 0.17 (a)	p = 0.203 (Chi^2 = 4.60)
δ^{15}N (‰)	1.39 ± 0.20 (a)	1.58 ± 0.29 (ab)	1.04 ± 0.21 (bc)	0.61 ± 0.26 (c)	**p < 0.0001** (F= 8.14)
Soil C (mg g^{-1} DW)	351.19 ± 15.53 (a)	63.33 ± 7.58 (c)	185.39 ± 19.29 (b)	202.80 ± 19.33 (b)	**p < 0.0001** (F = 63.24)
Soil N (mg g^{-1} DW)	18.42 ± 1.03 (a)	3.65 ± 0.40 (c)	10.11 ± 1.09 (b)	10.95 ± 0.89 (b)	**p < 0.0001** (Chi^2 = 50.12)
Soil P (mg g^{-1} DW)	0.73 ± 0.05 (*int) [n=34]	0.46 ± 0.05 (*int) [n=13]	0.54 ± 0.07 (*int)	0.49 ± 0.04 (*int)	**p < 0.0001** (F = 10.92)
Soil C:N	20.69 ± 1.57 (a)	17.41 ± 0.91 (a)	18.64 ± 0.59 (a)	18.24 ± 0.44 (a)	p = 0.375 (Chi^2 = 3.11)
Soil C:P	590.98 ± 64.14 (a) [n=34]	158.62 ± 16.14 (b) [n=13]	374.08 ± 38.28 (a)	479.85 ± 62.08 (a)	**p < 0.0001** (F = 23.11)
Soil N:P	31.67 ± 3.73 (a) [n=34]	8.80 ± 0.70 (b) [n=13]	20.07 ± 1.92 (a)	26.06 ± 3.37 (a)	**p < 0.0001** (F = 28.66)
DOC (µg g^{-1} DW)	739.61 ± 68.61 (a)	59.74 ± 5.07 (c)	173.95 ± 25.55 (b)	265.52 ± 46.41 (b)	**p < 0.0001** (Chi^2 = 54.21)
TDN (µg g^{-1} DW)	50.36 ± 7.52 (a)	4.04 ± 0.74 (c)	15.54 ± 2.63 (b)	26.16 ± 4.82 (b)	**p < 0.0001** (F = 44.92)
DOC:TDN	22.13 ± 3.19 (a)	22.16 ± 3.83 (a)	13.19 ± 1.69 (b)	11.43 ± 1.07 (b)	**p < 0.0001** (F = 8.22)

*Presented are means ± SE (organic: n = 35; mineral: n = 14; cryoturbated: n = 13, permafrost: n = 19; with deviations noted in the table). Statistical results from linear mixed-effects models (Type II ANOVA; p-values and F-statistics) are shown in the right column. When model assumptions were not met, Kruskal Wallis tests were applied (p-values and Chi² statistics). Pairwise comparisons (Tukey-adjusted estimated marginal means or Bonferroni-adjusted pairwise Wilcoxon tests) are indicated by letter groupings in brackets. Significant interactions between polygon type and soil layer are marked with (*int).* ***Interactive effects:*** *In LCPs, soil layers had similar soil P concentrations, while in FCPs and HCPs, the organic layer had higher P concentrations compared to the mineral and permafrost layers (LME: p = 0.049, F = 2.4; pairwise comparisons for the organic vs. mineral layer: FCP: p = 0.0002, t = 4.6; HCP: p = 0.0017, t = 3.9; and the organic vs. permafrost layer: FCP: p = 0.063, t = 2.6; HCP: p = 0.005, t = 3.5). Abbreviations: SWC = soil water content, DOC = dissolved organic carbon, TDN = total dissolved nitrogen; HCPs = high-centered-, FCPs = flat-centered-, LCPs = low-centered polygons.*

S3. Chemical composition of soil organic matter

We used Pyrolysis- GC/MS for obtaining characteristic fingerprints of the chemical composition of the soil organic matter pools among the investigated ice-wedge polygon types and soil layer categories. Therefore, we used a semi-automated approach as explained in Martin et al., (2024), with minor adaptations.

Approximately 0.1 to 0.2 mg of dried and finely milled soil samples were weighed into pyrolysis glass tubes (constricted Quartz Tubes for 6000 DISC and Autosampler, CDS Analytical) deploying a randomized sample order. Ideal sample amounts (adapted to respective soil C concentrations) were determined in pre-tests. We compiled a mixed reference sample out of four randomly selected samples, representing different soil layers, polygon types and sampling areas. To ensure consistent quality of the instruments' performance throughout the runs we included multiple technical replicates of an external soil standard (IHSS Elliott Soil Humic Acid Standard IV) as well as for the mixed reference sample. To account for possible contamination of the glass tubes, we included several blanks throughout the sample sequence. Samples were pyrolyzed (Pyroprobe 6200 and Autosampler 6250T, CDS) at an initial temperature of 50 °C (5 sec) followed by a ramp increase of 20 °C/sec and a final temperature of 600 °C (20 sec). Pyrolysis products were transferred into the GC-TOF-MS system (Pegasus BT GC-MS, LECO) with a constant target flow of 1mL helium/min at 280 °C. After each sample the pyrolysis chamber was heated to 1,000 °C for 60 seconds and flushed clean for the next sample. A polar column (Supelcowax TM 10 Fused Silica Capillary Column, 30 m x 0.25 mm x 0.25 µm film thickness, Sigma-Aldrich) was used. The GC was kept at 50 °C (2 min), followed by an increase of 7 °C/min until reaching the final temperature of 250 °C (5 min). All resulting chromatograms were analyzed with ChromaTOF software (version 5.51.50.068774, LECO).

After visually checking the regularity of the chromatograms from the three technical replicates of the mixed reference sample, one was selected for subsequent manual analysis and creation of a so-called "reference sample compound library". Therefore, we compared the mass spectrum of each individual peak within the chromatogram to suggested spectra from the electron ionization (EI) mass spectral libraries "mainlib" and "replib", contained in the NIST Library of Mass Spectrometry (U.S. Department of Commerce National Institute of Standards and Technology). Prior to confirming the identity of an individual substance, we additionally consulted (i) the fit to in literature reported retention times, (ii) revised the substances' relative position within a sequence of other identified compounds (this is particularly helpful for long-chained alkanes) and (iii) compared the in ChromaTOF included probability assessment of the observed ion m/z versus expected ion m/z. Following this process, we obtained a list of identified (e.g., "1-Dodecene") compounds plus compounds which we could not clearly assign to an entry from the NIST libraries, but which we could identify via their unique mass spectrum (e.g., "Peak_1").

From this data, we created a library of pyrolysis products that was employed for the subsequent semi-automated analysis of all samples and blanks. Hence, only substances that were included in the library were considered for the subsequent steps. Since this library of pyrolysis products is project specific, it

holds representative characteristics of the SOM pool of the respective sampling area. We employed the library-matching algorithm implemented in ChromaTOF and performed an automated targeted compound search for all compounds contained in the library. In this manner, we could reference substances within samples and blanks to those of the library. The m/z spectrum of every peak within an extracted- ion sample chromatogram (XIC) was compared to the deconvoluted spectrum of the substance from the library. A similarity match score (min. score = 1, max. score= 1000) provided information about the respective fit of the match. For the process of automated hit assignment, we set the minimum similarity match threshold to > 700 (the reliability of this threshold was evaluated during pre-tests in the phase of method development). Further, we set the threshold of the min. peak signal to noise ratio (S/N) >100 to remove background noise within the chromatograms (see also 10.5281/zenodo.18631833. After completion of the automated assignments via the algorithm, we manually checked the correctness of the automatically matched pyrolysis substances (e.g., "1-Dodecene", "Peak_1") by visual assessment and corrected wrong assignments. Such manual confirmation avoids wrong assignments due to very similar spectra (such as i.e., found with long-chained alkanes), but also allows to include the small fraction of compounds into the dataset, where manual identification is possible, but where the automatic matching algorithm failed (due to not meeting the similarity-threshold-criterium). Following these steps, we derived a presence-absence list from all pyrolysis products listed in the library ("1-Dodecene", "Peak_1"), plus their corresponding peak areas from all soil samples and blanks. To control for possible contamination in the pyrolysis system or the glass tubes, a blank correction step was performed on the dataset. Therefore, we subtracted mean areas of substances found in blanks from the area of the respective substance within the samples. Further, we normalized the sample chromatogram peak areas with respective soil carbon contents and the pyrolyzed amount of sample, as both factors can influence peak area and baseline height. Following the assumption that the sum of all pyrolysis-product-areas within a sample equals its carbon content, allowed us to calculate individual substance abundances (mg C g^{-1} soil DW).

We employed the phyloseq" package (McMurdie and Holmes, 2013) for handling the dataset, with (i) substance abundances being equivalent to the OTU-abundance matrix, (ii) SOM compound group classification being equivalent to taxonomic information, and (iii) metadata including information on polygon type and soil layer category. We excluded rare pyrolysis compounds accounting for less than 0.1 % of the total C content per sample. This step helped to reduce the size of the dataset by identifying those substances with a significant contribution to the respective overall sample peak area. From a total of 1387 pyrolysis products in the initial dataset, 534 were consequentially considered for the final SOM fingerprint.

We assigned these 534 pyrolysis products to the following SOM compound groups: (1) "aromatics & phenols [n=51]", (2) "carbohydrates" [n=48], (3) "N-containing compounds" [n=42], (4) "lignin-derived compounds" [n=16], and (5) "lipids" [n=68], with the classification being supported by literature (Buurman et al., 2005; González-Pérez et al., 2012; Hempfling and Schulten, 1990; Ninnes et al., 2017; Said et al., 2015; Saiz-Jimenez and De Leeuw, 1986; Schulten and Schnitzer, 1997; Shen et al., 2018; Stewart, 2012; Tolu et al., 2015; Vancampenhout et al., 2009). In case of no available literature

reference, we assigned the compound to one of the mentioned SOM groups based on their molecular structure, employing the US National Library of Medicine (NCBI) PubChem compound database (Kim et al., 2023). We summarized substances that we could not assign to one of the aforementioned compound groups (e.g., “Cyclononasiloxane“), plus all compounds that were matched to a nameless substance in the library (e.g., “Peak_1”) in a group that we called (6) “general & unknown compounds” [n=309]. A detailed list of all considered pyrolysis products (n = 534) and their assignment to SOM compound groups is available under 10.5281/zenodo.18631833.

Table S3. *Correlations between soil organic matter (SOM) compound group abundances and soil carbon content.*

Compound Class (mg C g^{-1} DW)	Soil C (mg g^{-1} DW)
Aromatics & Phenols	ρ (79) = 0.92; **p < 0.0001**
Carbohydrates	ρ (79) = 0.95; **p < 0.0001**
General & Unknown	ρ (79) = 0.92; **p < 0.0001**
Lignins	ρ (79) = 0.77; **p < 0.0001**
Lipids	ρ (79) = 0.90; **p < 0.0001**
N- Containing	ρ (79) = 0.98; **p < 0.0001**

Presented are Spearman’s rank-order correlation coefficients (ρ) with corresponding degrees of freedom (df) and two-sided p-values.

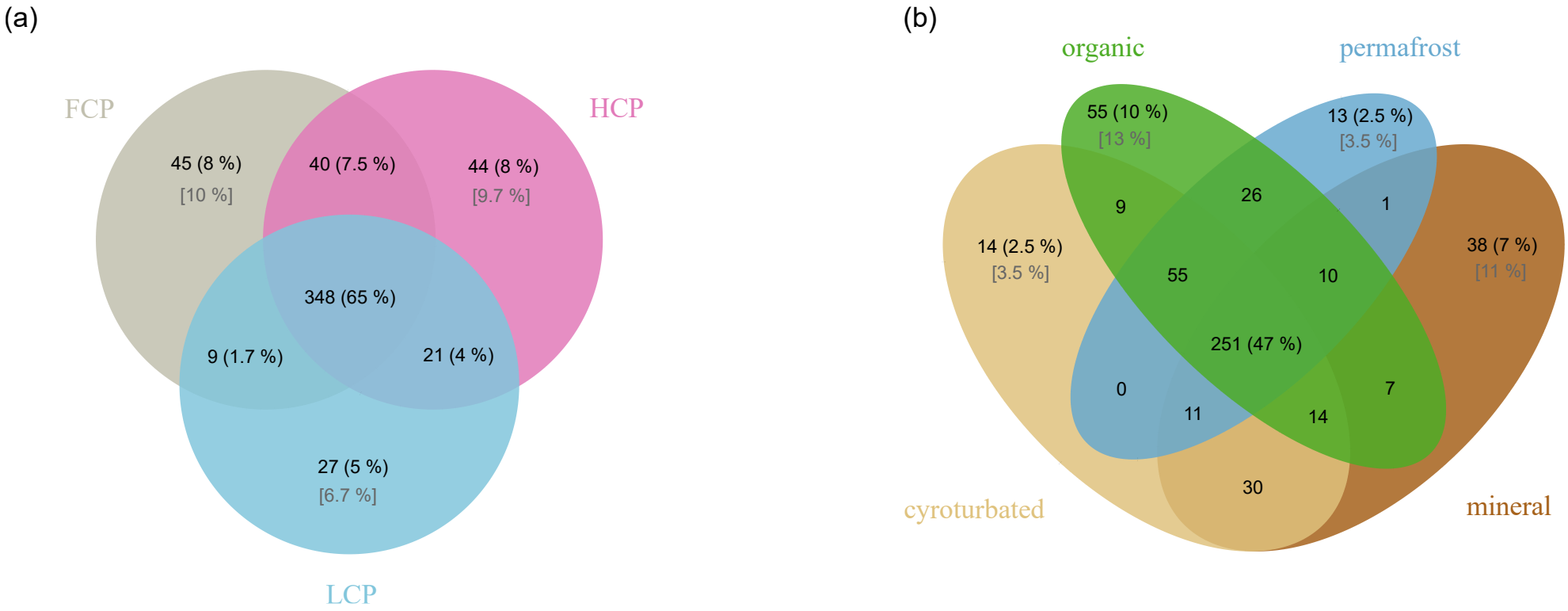

Figure S2. *Venn Diagrams depicting the number of shared and unique pyrolysis products among* ***(a)*** *ice-wedge polygon types (low-centered polygon, LCP, n = 20; flat-centered polygon, FCP, n = 32; high-centered polygon, HCP, n = 29), and* ***(b)*** *soil layers (organic topsoil, n = 35; mineral subsoil, n = 14; cryoturbated material, n = 13; permafrost, n = 19). Fractions of shared and unique pyrolysis products relative to the total number of substances (n = 534) are shown as percentages (%; black). The proportion of polygon-specific or soil layer-specific pyrolysis products relative to the number of pyrolysis products within each polygon type or soil layer are given in [%; grey].*

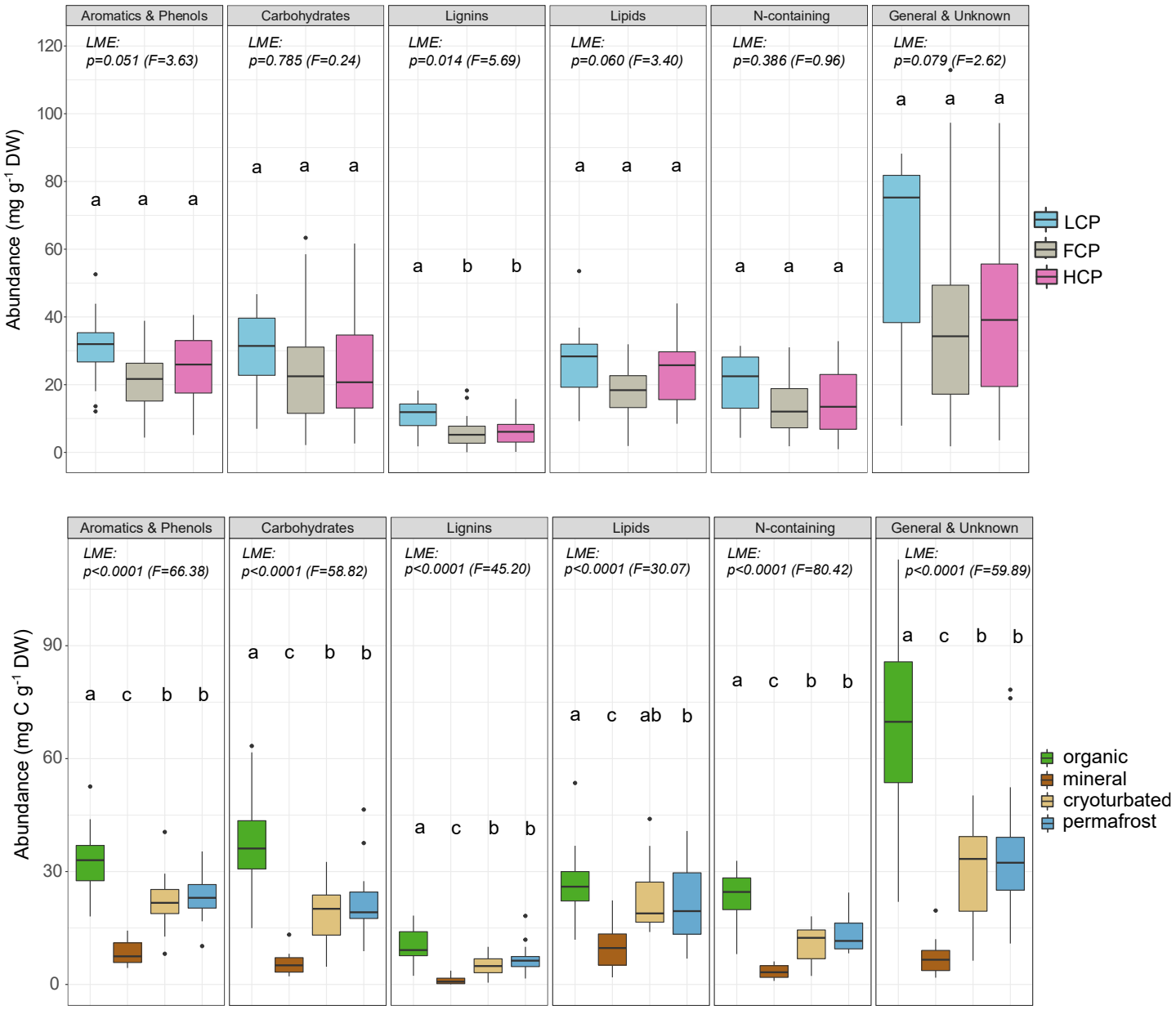

Figure S3. *Abundances (mg g^{-1} DW soil) of soil organic matter (SOM) compound groups across* ***(a)*** *ice-wedge polygon types (low-centered polygon, LCP, n = 20; flat-centered polygon, FCP, n = 32; high-centered polygon, HCP, n = 29) and across* ***(b)*** *soil layers (organic topsoil, n = 35; mineral subsoil, n = 14; cryoturbated material, n = 13; permafrost, n = 19). Statistical results from linear mixed-effects models (Type II ANOVA; p-values and F-statistics) are shown in respective panels. Results from pairwise comparisons (Tukey-adjusted estimated marginal means) are indicated by letter groupings. No interactive effects between polygon type and soil layer were observed.*

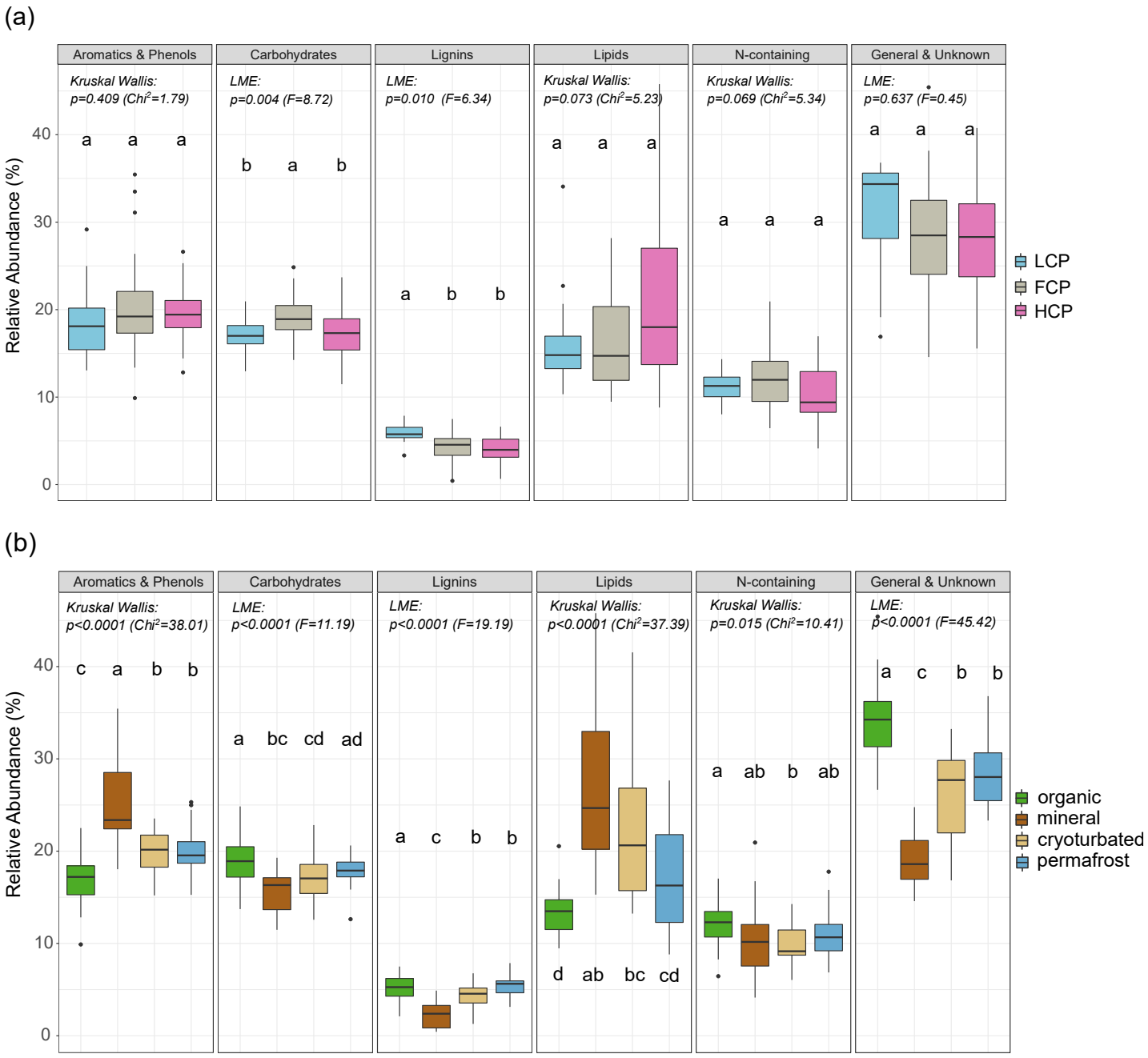

Figure S4. *Relative abundances (%) of soil organic matter (SOM) compound groups across* ***(a)*** *ice-wedge polygon types (low-centered polygon, LCP, n = 20; flat-centered polygon, FCP, n = 32; high-centered polygon, HCP, n = 29) and across* ***(b)*** *soil layers (organic topsoil, n = 35; mineral subsoil, n = 14; cryoturbated material, n = 13; permafrost, n = 19). Statistical results from linear mixed-effects models (Type II ANOVA; p-values and F-statistics) are shown in respective panels. When model assumptions were not met, Kruskal–Wallis tests were applied (p-values and Chi² statistics). Results from pairwise comparisons (Tukey-adjusted estimated marginal means or Bonferroni-adjusted pairwise Wilcoxon tests) are indicated by letter groupings in brackets. No interactive effects between polygon type and soil layer were observed.*

S4. Soil microbial communities

In this study, 'microbial communities' specifically refers to bacterial, archaeal, and fungal taxa profiled by amplicon sequencing the V4 region of the 16S rRNA gene and the ITS1 region, as these groups represent the primary decomposers in permafrost-affected soils. Despite their ecological relevance, we did not include groups such as micro-eukaryotes and viruses, as their consideration would have required alternative workflows (e.g., metagenomics or metatranscriptomics)

We extracted microbial DNA using the FastDNA™ SPIN Kit for Soil (MP Biomedicals, Santa Ana, USA) following the manufacturers' instructions but with minor modifications for cleaning the samples from the RNAlater™ Stabilization Solution. For cleaning, we added 1 ml sodium phosphate buffer (contained in the kit) and vortexed gently. After a short centrifugation step, we discarded the supernatant without disturbing the soil pellet and repeated the procedure five consecutive times. Subsequently, we followed the conventional DNA extraction protocol. Due to the large differences in bulk density, soil C and the assumed discrepancy in microbial biomass between the organic layer and the other layers, we used 250 mg FW soil from the organic topsoil and 400 mg FW soil from all other soil layers respectively. To control for potential contamination, extraction blanks were included and subjected to subsequent quantification and sequencing steps. DNA extracts were treated with the OneStep PCR Inhibitor Removal Kit (Zymo Research, Irvine, CA, USA) to remove possibly occurring inhibitory polyphenolics, humic- and fulvic acids, and tannins. DNA concentrations were quantified using the Quant-iT ™ PicoGreen® dsDNA Assay Kit (Thermo Fisher Scientific, Waltham, USA).

Amplicon sequencing and raw data processing was performed at the Joint Microbiome Facility of the Medical University of Vienna and the University of Vienna (JMF project ID JMF-2008-5). Datasets are deposited in the NCBI Sequence Read Archive under BioProject accession number (PRJNA1274918). We used DNA extracts that have been normalized to a concentration of 0.5 ng μl^{-1} (no sample required concentration; dilution factors ranged between 18 ± 5 (mean ± stderr) for samples from permafrost, 27 ± 4 from mineral, 48 ±10 for cryoturbated, and 45 ± 5 for organic topsoil layers). This normalization step accounts for variation in extraction yields due to differential biomass and dilutes potential PCR inhibitors in addition.

A two-step barcoding approach was employed to generate amplicon libraries of archaeal, bacterial, and fungal communities using Illumina MiSeq (V3 Kit; 2 x 300 bp configuration, 1% PhiX spike-in), following (Pjevac et al., 2021). The V4 hypervariable region of the 16S rRNA gene was amplified using primer pairs 515F (GTGYCAGCMGCCGCGGTAA, (Parada et al., 2016)) and 806R (GGACTACNVGGGTWTCTAAT, (Apprill et al., 2015)). The fungal ITS1 region was amplified using primer pairs ITS1F (CTTGGTCATTTAGAGGAAGTAA, (Smith and Peay, 2014)) and ITS2 (GCTGCGTTCTTCATCGATGC, (White et al., 1990)). We note that applying ASV-based approaches to fungal ITS regions may be affected by high sequence variability and intra-genomic variation, potentially influencing taxonomic resolution.

First-step 25 µl PCR reactions consisted of 1x DreamTaq Green PCR master mix, 0.1 µg μl^{-1} BSA, 0.25 µmol l^{-1} of each headed primer, and 2 µl of DNA template. We used the following amplification conditions:

- 16S rRNA gene: initial denaturation at 94 °C for 3 min, followed by 30 cycles of 94 °C for 45 s, 52 °C for 60 s and 72 °C for 60 s, and final elongation at 72 °C for 10 min.
- ITS1 region: 94 °C for 1 min, 35 cycles of 94 °C for 45 s, 52 °C for 60 s and 72 °C for 90 s, followed by final elongation at 72 °C for 10 min.

Datasets were deposited in the NCBI Sequence Read Archive under BioProject accession number (PRJNA1274918). The original sequencing data is also accessible under 10.5281/zenodo.18631833.

Prior downstream analyses, we cleaned the amplicon sequencing datasets from non-archaeal, -bacterial, or -fungal sequences and excluded samples with less than 500 obtained reads (exclusion of two samples from the 16S rRNA, and exclusion of 3 samples from the ITS1 datasets, respectively). Contaminant sequences were removed on an ASV-specific basis by subtracting the highest observed read number in one of the DNA extraction blanks from the corresponding sample reads (resulting read distributions were carefully investigated). To standardize sequencing depth across samples, we rarefied these datasets (using the rarefy_even_depth()-function implemented in phyloseq with replacement-argument ==F; and determined cut-offs at 2650 16S rRNA reads and at 543 ITS1 reads, respectively). We assessed α-diversity as richness (number of observed ASVs) and Shannon diversity. We note that α-diversity estimates based on fungal ITS ASVs may be inflated due to intra-genomic and intra-specific variability and should therefore be interpreted with caution.

Digital droplet PCR (ddPCR) was performed to quantify 16S rRNA genes and ITS1 regions with the same primers used for sequencing. Each ddPCR reaction had a volume of 22 µL and consisted of 1x QX200 ddPCR EvaGreen Supermix (BioRad), 0.1 µmol L^{-1} of each primer and 0.05 and 0.025 ng of template for the quantification of 16S rRNA genes and ITS1 regions, respectively. Droplets were generated on a QX200 ™ Droplet Generator (BioRad) and immediately subjected to PCR amplification (amplification conditions in Table S4). PCR products in droplets were kept at 4 °C over night to increase their separation before measuring their fluorescence intensity on a QX200 ™ Droplet Reader (BioRad). Gene copy numbers were calculated using the QX ONE Software Standard Edition (v. 1.2, BioRad) where thresholds between positive and negative droplet populations were set consistently for each sample using the histogram as a guide. We expressed final ddPCR results as 16S rRNA and ITS1 gene copy numbers g^{-1} DW soil and used them as abundance proxies for bacteria and archaea, and fungi, respectively. We note that we did not explicitly correct for taxon-specific ribosomal gene copy number variation, and that ddPCR-derived abundance estimates therefore do not directly reflect microbial cell numbers.

Table S4. *Cycling conditions used for digital droplet PCR (ddPCR) amplification of 16S rRNA genes and ITS1 regions, including temperature steps, cycle numbers, and reaction parameters.*

Temperature	***Time***	***Cycles***	***Details***	***Comments***
16S rRNA ddPCR quantification conditions				
95 °C	5 min			add a temperature ramp of 2 °C/second to all steps
95 °C	30 s	x 5	-1 °C every cycle	
57 °C	120 s			
95 °C	30 s	x 35		
52 °C	120 s			
4 °C	5 min			
90 °C	5 min			
4 °C	hold			

Temperature	***Time***	***Cycles***	***Details***	***Comments***
ITS1 Region ddPCR quantification conditions				
95 °C	5 min			add a temperature ramp of 2°C/second to all steps
95 °C	30 s	x 5	-1 °C every cycle	
60 °C	120 s			
95 °C	30 s	x 35		
55 °C	120 s			
4 °C	5 min			
90 °C	5 min			
4 °C	hold			

To derive ddPCR-informed abundance estimates, we followed the framework of quantitative microbiome profiling (Vandeputte et al., 2017), in which amplicon-based relative abundances are scaled using gene copy numbers. Accordingly, we calculated ASV-level abundance estimates (gene copy number corrected reads per g soil DW) by multiplying the 16S rRNA or ITS1 gene copy numbers measured in ddPCR assays with their respective relative abundances from the amplicon sequencing datasets (based on the raw reads-dataset after removal of non-archaeal, -bacterial, or -fungal

sequences, exclusion of samples with less than 500 obtained reads, and blank-correction). In the next step, we excluded rare bacterial, archaeal, and fungal taxa (defined as containing less than 0.05 % of all gene copy number corrected reads per sample), which resulted in 3643 bacterial and 137 archaeal ASVs (classified into 47 phyla, 111 classes, 201 orders, 247 families, and 308 genera) and 1604 fungal ASVs (classified into 7 phyla, 19 classes, 44 orders, 77 families and 101 genera) being considered in the follow-up analyses. of certain phyla (ddPCR-corrected reads per g DW aggregated on phylum level) between polygon types and soil layer categories. The data is accessible under 10.5281/zenodo.18631833.

To visualize microbial community composition (β-diversity) we followed a widely acknowledged approach for handling compositional data (e.g., Alteio et al., 2021; Barlow et al., 2020; Gloor et al., 2017). For this, we performed Principal Component Analysis (PCA) on center-log-ratio-(clr-) transformed gene copy number corrected reads g-1 DW (corresponds to Aitchison distance, Aitchison, 1984).

We explored potential ecological roles of fungal communities using the FungalTraits database (Põlme et al., 2020). To balance ecological interpretability and assignment confidence, we performed trait-based annotations at the genus level, since higher taxonomic ranks often encompass multiple or ambiguous ecological strategies. Using this approach, approximately 18 % of fungal ASVs in the dataset could be reliably assigned to functional guilds (82 % remained unclassified). Most prevalent on the dataset were ectomycorrhizal fungi (6.4 %) and saprotrophs (7.7 %) (encompassing litter-, wood-, and soil-associated taxa), followed by root endophytes (1 %). Several additional lifestyles (e.g., parasitic, lichenized, pathogenic, or specialized saprotrophic fungi) were present but contributed less than 1 % each. Summary tables of the FungalTraits database assignments including the differential distribution of guilds across polygon types and soil layers are accessible under 10.5281/zenodo.18631833.

S4.1. Bacterial and archaeal communities

Table S5. *Interactive effects of polygon type and soil layer category on bacterial and archaeal community composition, based on PERMANOVA analyses corresponding to Figure 3. Reported are Bonferroni-adjusted p-values and F-statistics. Only significant results are shown.*

Comparison	Result	Test
organic layer across all polygon types	p=0.001 (F=4.33)	PERMANOVA
LCP vs. FCP	p=0.003 (F=5.29)	Pairwise PERMANOVA
LCP vs. HCP	p=0.003 (F=7.16)	
mineral layer across all polygon types	p=0.067 (F=1.64)	PERMANOVA
cryoturbated layer across all polygon types	p=0.114 (F=1.54)	PERMANOVA
permafrost layer across all polygon types	p=0.008 (F=1.57)	PERMANOVA
LCP vs. FCP	p=0.003 (F=2.09)	Pairwise PERMANOVA
soil layers within LCPs	p=0.003 (F=2.24)	PERMANOVA
organic vs. permafrost	p=0.006 (F=3.37)	Pairwise PERMANOVA
soil layers within FCPs	p=0.001 (F=2.65)	PERMANOVA
organic vs. cryoturbated	p=0.006 (F=2.80)	Pairwise PERMANOVA
organic vs. permafrost	p=0.006 (F=4.59)	
soil layers within HCPs	p=0.001 (F=3.80)	PERMANOVA
organic vs. mineral	p=0.006 (F=3.94)	Pairwise PERMANOVA
organic vs. cryoturbated	p=0.006 (F=4.06)	
organic vs. permafrost	p=0.006 (F=5.71)	
mineral vs. permafrost	p=0.024 (F=3.13)	
cryoturbated vs. permafrost	p=0.018 (F=2.66)	

Table S6. *ddPCR-informed abundance estimates (gene copy number corrected reads g^{-1} DW soil) of selected bacterial and archaeal phyla across soil layers per ice-wedge polygon type.*

	Soil Layer	LCP	FCP	HCP	Polygon effect	Soil layer effect	Interactive effect
Acidobacteriota	organic	$2.54\ e^{8} \pm 1.07\ e^{8}$	$7.27\ e^{8} \pm 1.34\ e^{8}$	$7.64\ e^{8} \pm 1.37\ e^{8}$	Kruskal Wallis: p=0.138; Chi^2=4.0	Kruskal Wallis: p<0.0001; Chi^2=42.0 Pairwise Wilcox: org-min: p<0.0001 org-cryo: p=0.004 org-perm: p<0.0001	Pairwise Wilcox organic: LCP-FCP: p=0.036 LCP-HCP: p=0.009 FCP-HCP: p=1.0
	mineral	$9.36\ e^{6} \pm 4.87\ e^{6}$	$4.11\ e^{7} \pm 9.96\ e^{6}$	$4.69\ e^{7} \pm 1.60\ e^{7}$			
	cryoturbated	-	$5.74\ e^{7} \pm 2.82\ e^{7}$	$1.07\ e^{8} \pm 4.04\ e^{7}$			
	permafrost	$6.53\ e^{6} \pm 3.09\ e^{6}$	$4.42\ e^{7} \pm 2.09\ e^{7}$	$2.02\ e^{7} \pm 1.11\ e^{7}$			
Actinobacteriota	organic	$7.62\ e^{7} \pm 2.43\ e^{7}$	$1.44\ e^{8} \pm 3.31\ e^{7}$	$1.29\ e^{8} \pm 2.10\ e^{7}$	LME: p=0.004; F=6.0 Emmeans pairwise: LCP-FCP: p=0.023 LCP-HCP: p=0.013 FCP-HCP: p=0.935	LME: p=0.0001; F=11.3 Emmeans pairwise: org-min: p=0.023 org-cryo: p=0.961 org-perm: p=0.030	
	mineral	$1.57\ e^{7} \pm 7.14\ e^{6}$	$2.18\ e^{7} \pm 9.05\ e^{6}$	$3.16\ e^{7} \pm 7.95\ e^{6}$			
	cryoturbated	-	$1.02\ e^{8} \pm 1.65\ e^{7}$	$1.76\ e^{8} \pm 2.39\ e^{7}$			
	permafrost	$2.06\ e^{7} \pm 8.05\ e^{6}$	$1.15\ e^{8} \pm 4.32\ e^{7}$	$6.45\ e^{7} \pm 2.77\ e^{7}$			
Armatimonadota	organic	$2.86\ e^{5} \pm 1.80\ e^{5}$	$3.19\ e^{6} \pm 1.04\ e^{6}$	$5.12\ e^{6} \pm 1.97\ e^{6}$	Kruskal Wallis: p=0.009; Chi^2=9.3 Pairwise Wilcox: LCP-FCP: p=0.008 LCP-HCP: p=0.097 FCP-HCP: p=0.990	Kruskal Wallis: p=0.772; Chi^2=1.1	
	mineral	$3.07\ e^{5} \pm 3.07\ e^{5}$	$1.37\ e^{6} \pm 4.41\ e^{5}$	$3.76\ e^{5} \pm 9.97\ e^{4}$			
	cryoturbated	-	$1.63\ e^{6} \pm 1.01\ e^{6}$	$4.99\ e^{5} \pm 2.34\ e^{5}$			
	permafrost	$4.65\ e^{5} \pm 2.47\ e^{5}$	$2.97e^{6} \pm 1.59\ e^{6}$	$7.53\ e^{5} \pm 4.86\ e^{5}$			
Bacteroidota	organic	$5.83\ e^{8} \pm 1.31\ e^{8}$	$1.06\ e^{9} \pm 2.36\ e^{8}$	$1.02\ e^{9} \pm 1.89\ e^{8}$	Kruskal Wallis: p=0.221; Chi^2=3.0	Kruskal-Wallis: p<0.0001; Chi^2=29.7 Pairwise Wilcox: org-min: p<0.0001 org-cryo: p=0.429 org-perm: 0.008	
	mineral	$7.06\ e^{7} \pm 4.17\ e^{7}$	$1.09\ e^{8} \pm 4.93\ e^{7}$	$1.15\ e^{8} \pm 4.54\ e^{7}$			
	cryoturbated	-	$6.94\ e^{8} \pm 2.20\ e^{8}$	$3.36\ e^{8} \pm 5.58\ e^{7}$			
	permafrost	$1.21\ e^{8} \pm 2.25\ e^{7}$	$6.26\ e^{8} \pm 1.46\ e^{8}$	$2.68\ e^{8} \pm 7.56\ e^{7}$			
Bdellovibrionota	organic	$1.83\ e^{6} \pm 1.13\ e^{6}$	$5.44\ e^{6} \pm 1.48\ e^{6}$	$4.79\ e^{6} \pm 2.05\ e^{6}$	Kruskal Wallis: p=0.0006; Chi^2=14.9	Kruskal Wallis: p=0.0002; Chi^2=14.9	
	mineral	$2.01\ e^{5} \pm 4.39\ e^{4}$	$1.51\ e^{6} \pm 1.16\ e^{6}$	$1.61\ e^{6} \pm 6.75\ e^{5}$			

	cryoturbated	-	8.90 e^6 ± 2.78 e^6	7.45 e^6 ± 2.19 e^6	Pairwise Wilcox: LCP-FCP: p<0.0001 LCP-HCP: p=0.016 FCP-HCP: p=0.904	cryo-min: p=0.003 cryo-perm: p=0.002	
	permafrost	2.75 e^4 ± 2.75 e^4	3.22 e^6 ± 8.21 e^5	1.15 e^6 ± 8.83 e^5			
Caldisericota	organic	3.69 e^5 ± 2.45 ^{e5}	0.00 ± 0.00	0.00 ± 0.00	Kruskal Wallis: p=0.007; Chi^2=10.0 Pairwise Wilcox LCP-FCP: p=0.076 LCP-HCP: p=0.010 FCP-HCP: p=1.00	Kruskal Wallis: p<0.0001; Chi^2=25.2 The permafrost layer harbored 81 % of ddPCR-corr. reads assigned to this phylum.	
	mineral	8.93 e^5 ± 2.10 e^5	2.58 e^5 ± 2.58 e^5	0.00 ± 0.00			
	cryoturbated	-	3.69 e^5 ± 2.26 e^5	0.00 ± 0.00			
	permafrost	1.25 e^6 ± 4.43 e^5	1.85 e^6 ± 1.04 e6	3.37 e^6 ± 1.91 e^6			
Campylobacterota	organic	0.00 ± 0.00	0.00 ± 0.00	0.00 ± 0.00		The permafrost layer harbored 93 % of ddPCR-corr. reads assigned to this phylum.	
	mineral	0.00 ± 0.00	0.00 ± 0.00	0.00 ± 0.00			
	cryoturbated	-	2.48 e^5 ± 2.48 e^5	0.00 ± 0.00			
	permafrost	3.83 e^5 ± 2.86 e^5	9.41 e^5 ± 4.78 e^5	1.20 e^6 ± 1.11 e^6			
Cloacimonadota	organic	5.06 e^5 ± 3.29 e^5	0.00 ± 0.00	0.00 ± 0.00		The permafrost layer harbored 68 % of ddPCR-corr. reads assigned to this phylum.	
	mineral	0.00 ± 0.00	3.02 e^4 ± 3.02 e^4	0.00 ± 0.00			
	cryoturbated	-	0.00 ± 0.00	0.00 ± 0.00			
	permafrost	9.01 e^5 ± 7.55 e^5	9.28 e^5 ± 7.28 e^5	2.08 e^5 ± 1.25 e^5			
Cyanobacteria	organic	6.00 e^5 ± 3.68 e^5	1.73 e^6 ± 1.03 e^6	4.98 e^6 ± 1.70 e^6	Kruskal Wallis: p=0.054; Chi^2=5.9	Kruskal Wallis: p=0.001; Chi^2=15.6 The permafrost layer harbored 1 % of ddPCR-corr. reads assigned to this phylum.	
	mineral	1.54 e^5 ± 9.11 e^4	2.46 e^5 ± 1.79 e^5	7.25 e^5 ± 3.85 e^5			
	cryoturbated	-	1.01 e^6 ± 5.02 e^5	3.06 e^6 ± 1.40 e^6			
	permafrost	0.00 ± 0.00	1.81 e^5 ± 1.81 e^5	0.00 ± 0.00			
Crenarchaeota	organic	9.69 e^6 ± 3.64 e^6	2.60 e^6 ± 2.04 e^6	0.00 ± 0.00	Kruskal Wallis: p<0.0001; Chi^2=21.4 Pairwise Wilcox: LCP-FCP: p=0.014 LCP-HCP: p<0.0001 FCP-HCP: p=0.131	Kruskal Wallis: p=0.249; Chi^2=4.12	Pairwise Wilcox - organic: LCP-FCP: p=0.049 LCP-HCP: p<0.0001 FCP-HCP: p=0.278
	mineral	2.63 e^4 ± 2.63 e^4	3.36 e^5 ± 2.00 e^5	6.23 e^4 ± 6.23 e^4			
	cryoturbated	-	9.07 e^4 ± 9.07 e^4	0.00 ± 0.00			
	permafrost	2.57 e^5 ± 1.45 e^5	9.62 e^4 ± 6.21 e^4	6.33 e^4 ± 4.06 e^4			

Desulfobacterota	organic mineral cryoturbated permafrost	2.04 e^8 ± 5.97 e^7 1.66 e^7 ± 8.41 e^6 - 1.41 e^7 ± 3.55 e^6	7.89 e^7 ± 3.32 e^7 4.26 e^7 ± 2.04 e^7 8.31 e^7 ± 2.23 e^7 6.10 e^7 ± 1.16 e^7	3.27 e^7 ± 1.25 e^7 1.27 e^7 ± 2.44 e^6 2.31 e^7 ± 7.15 e^6 2.05 e^7 ± 4.44 e^6	Kruskal Wallis: p=0.026; Chi^2=7.3 Pairwise Wilcox: LCP-FCP: p=1.000 LCP-HCP: p=0.056 FCP-HCP: p=0.088	Kruskal Wallis: p=0.286; Chi^2=3.8	Pairwise Wilcox - organic: LCP-FCP: p=0.207 LCP- HCP: p=0.018 FCP-HCP: p=1.0
Euryarchaeota	organic mineral cryoturbated permafrost	8.11 e^7 ± 3.29 e^7 3.52 e5 ± 1.59 e^4 - 1.34 e^6 ± 4.72 e^5	9.61 e^6 ± 6.85 e^6 5.00 e^5 ± 2.66 e^5 1.11 e^6 ± 5.09 e^5 3.29 e^6 ± 1.46 e^6	3.00 e^5 ± 3.00 e^5 1.17 e^6 ± 5.67 e^5 1.29 e^6 ± 8.22 e^5 1.67 e^6 ± 1.27 e^6	Kruskal Wallis: p<0.0001; Chi^2=17.7 Pairwise Wilcox: LCP-FCP: p=0.005 LCP-HCP: p<0.0001 FCP-HCP: p=0.972	Kruskal Wallis: p=0.617; Chi^2=1.8	Pairwise Wilcox organic: LCP-FCP: p=0.006 LCP-HCP: p<0.0001 FCP-HCP: p=0.853
Firmicutes	organic mineral cryoturbated permafrost	1.24 e^7 ± 2.45 e^6 4.91 e^6 ± 3.30 e^6 - 2.30 e^7 ± 5.37 e^6	6.97 e^6 ± 2.34 e^6 5.40 e^6 ± 2.42 e^6 1.67 e^7 ± 7.69 e^6 3.69 e^7 ± 1.25 e^7	5.53 e^6 ± 1.43 e^6 1.70 e^6 ± 8.04 e^5 5.08 e^6 ± 1.40 e^6 2.34 e^7 ± 6.21 e^6	Kruskal Wallis: p=0.063; Chi^2=5.5	Kruskal Wallis: p<0.0001; Chi^2=22.5 Pairwise Wilcox: perm-org: p<0.0001 perm-min: p<0.0001 perm-cryo: p=0.067	
Gemmatimonadota	organic mineral cryoturbated permafrost	4.74 e^4 ± 4.74 e^4 4.73 e^4 ± 4.73 e^4 - 0.00 ± 0.00	1.23 e^7 ± 3.55 e^6 3.96 e^6 ± 1.14 e^6 3.41 e^7 ± 2.3 e^7 1.39 e^7 ± 9.38 e^6	2.96 e^7 ± 6.59 e^6 8.22 e^6 ± 3.78 e^6 1.93 e^7 ± 4.71 e^6 1.63 e^6 ± 9.88 e^5	Kruskal Wallis: p<0.0001; Chi^2=34.6 Pairwise Wilcox: LCP-FCP: p<0.0001 LCP-HCP: p<0.0001 FCP-HCP: p=1.0	Kruskal Wallis: p=0.013; Chi^2=10.7	Pairwise Wilcox permafrost: LCP-FCP: p=0.02 LCP-HCP: p=0.22 FCP-HCP: p=0.25 organic: LCP-FCP: p=0.0007 LCP-HCP: p=0.0003 FCP-HCP: p=0.227
Halobacterota	organic mineral cryoturbated permafrost	1.36 e^7 ± 2.57 e^6 4.00 e^6 ± 1.52 e^6 - 4.22 e^6 ± 1.86 e^6	9.75 e^5 ± 7.23 e^5 1.89 e^6 ± 1.51 e^6 5.29 e^6 ± 2.72 e^6 4.03 e^6 ± 1.80 e^6	1.42 e^5 ± 1.42 e^5 1.84 e^6 ± 1.42 e^6 4.40 e^6 ± 1.18 e^6 5.09 e^6 ± 1.37 e^6	Kruskal Wallis: p<0.0001; Chi^2=20.5 Pairwise Wilcox: LCP-FCP: p<0.0001 LCP-HCP: p<0.0001 FCP-HCP: p=1.0	Kruskal Wallis: p=0.048; Chi^2=7.9 org-perm in LCP: p=0.083 in FCP: p=0.032 in HCP: p=0.002	Pairwise Wilcox organic: LCP-FCP: p<0.0001 LCP-HCP: p<0.0001 FCP-HCP: p=1.0
Latescibacterota	organic mineral	8.54 e^6 ± 3.95 e^6 3.07 e^5 ± 3.07 e^5	0.00 ± 0.00 5.50 e^4 ± 3.81 e^4	1.22 e^6 ± 9.36 e^5 0.00 ± 0.00			LCP organic harbored 88 % of ddPCR-corr.

	cryoturbated	-	0.00 ± 0.00	0.00 ± 0.00			reads assigned to this phylum
	permafrost	1.10 e^4 ± 1.10 e^4	0.00 ± 0.00	0.00 ± 0.00			
Methylomirabilota	organic	4.04 e^6 ± 8.17 e^5	2.12 e^6 ± 1.71 e^6	3.24 e^5 ± 3.24 e^5	Kruskal Wallis: p=0.708; Chi^2=0.7	Kruskal Wallis: p=0.016; Chi^2=8.3 The permafrost layer harbored < 1 % of ddPCR-corr. reads assigned to this phylum.	LCP organic harbored 60 % of ddPCR-corr. reads assigned to this phylum
	mineral	2.10 e^5 ± 1.58 e^5	2.13 e^5 ± 1.54 e^5	1.24 e^5 ± 8.18 e^4			
	cryoturbated	-	0.00 ± 0.00	0.00 ± 0.00			
	permafrost	1.18 e^5 ± 7.52 e^4	0.00 ± 0.00	0.00 ± 0.00			
Micrarchaeota	organic	2.57 e^6 ± 9.44 e^5	1.17 e^6 ± 1.17 e^6	0.00 ± 0.00			LCP organic harbored 69 % of ddPCR-corr. reads assigned to this phylum
	mineral	0.00 ± 0.00	0.00 ± 0.00	0.00 ± 0.00			
	cryoturbated	-	0.00 ± 0.00	0.00 ± 0.00			
	permafrost	0.00 ± 0.00	0.00 ± 0.00	0.00 ± 0.00			
Myxococcota	organic	9.63 e^6 ± 6.20 e^6	2.71 e^7 ± 7.93 e^6	3.59 e^7 ± 5.74 e^6	Kruskal Wallis: p=0.106; Chi^2=4.5	Kruskal Wallis: p<0.0001; Chi^2=41.4 org-perm in LCP: p=0.047 in FCP: p=0.008 in HCP: p=0.005	Pairwise Wilcox organic: LCP-FCP: p=0.104 LCP-HCP: p=0.007 FCP-HCP: p=0.765
	mineral	1.91 e^5 ± 5.44 e^4	1.25 e^5 ± 1.11 e^5	1.58 e^6 ± 6.00 e^5			
	cryoturbated	-	1.68 e^6 ± 8.45 e^5	2.83 e^6 ± 7.48 e^5			
	permafrost	0.00 ± 0.00	6.73 e^5 ± 6.73 e^5	0.00 ± 0.00			
Nanoarchaeota	organic	4.56 e^7 ± 1.47 e^7	3.03 e^7 ± 1.34 e^7	6.63 e^5 ± 4.58 e^5	Kruskal Wallis: p<0.0001; Chi^2=21.3 Pairwise Wilcox: LCP-FCP: p=0.220 LCP-HCP: p<0.0001 FCP-HCP: p=0.001	Kruskal Wallis: p=0.369; Chi^2=3.2	LCP organic harbored 48 % of ddPCR-corr. reads assigned to this phylum.
	mineral	1.93 e^6 ± 1.87 e^6	1.83 e^6 ± 1.09 e^6	5.80 e^5 ± 3.89 e^5			
	cryoturbated	-	1.87 e^7 ± 8.03 e^6	8.24 e^5 ± 6.60 e^5			
	permafrost	1.85 e^6 ± 7.68 e^5	1.26 e^7 ± 8.25 e^6	4.87 e^5 ± 2.10 e^5			
Patescibacteria	organic	4.81 e^7 ± 1.00 e^7	2.55 e^7 ± 9.85 e^6	1.15 e^7 ± 3.84 e^6	LME: p=0.175; F=1.9	LME: p=0.001; F=5.9	LME: p=0.014; F=3.2 Emmeans pairwise organic: LCP-FCP: p=0.211 LCP-HCP: p=0.009 FCP-HCP: p=0.320
	mineral	4.46 e^6 ± 6.95 e^5	1.52 e^7 ± 8.10 e^6	1.71 e^7 ± 1.03 e^7			
	cryoturbated	-	7.14 e^7 ± 2.35 e^7	4.54 e^7 ± 1.22 e^7			
	permafrost	1.17 e^7 ± 5.39 e^6	5.00 e^7 ± 1.01 e^7	1.52 e^7 ± 3.66 e^6			

Planctomycetota	organic mineral cryoturbated permafrost	1.53 e^7 ± 5.40 e^6 0.00 ± 0.00 - 1.32 e^5 ± 1.07 e^5	5.21 e^7 ± 1.69 e^7 1.49 e^6 ± 5.60 e^5 4.92 e^6 ± 2.93 e^6 1.65 e^6 ± 8.07 e^5	5.15 e^7 ± 8.91 e^6 2.47 e^6 ± 1.21 e^6 4.63 e^6 ± 1.92 e^6 1.06 e^6 ± 9.46 e^5	Kruskal Wallis: p=0.181; Chi^2=3.4	Kruskal Wallis: p<0.0001; Chi^2=41.1	Pairwise Wilcox - organic: LCP-FCP: p=0.235 LCP-HCP: p=0.005 FCP-HCP: p=1.0
Proteobacteria	organic mineral cryoturbated permafrost	2.45 e^8 ± 7.11 e^7 7.07 e^6 ± 2.06 e^5 - 9.90 e^7 ± 4.57 e^7	7.06 e^8 ± 1.40 e^8 6.16 e^7 ± 2.44 e^7 4.89 e^8 ± 3.21 e^8 3.27 e^8 ± 9.45 e^7	8.26 e^8 ± 1.77 e^8 1.42 e^8 ± 3.47 e^7 4.29 e^8 ± 9.87 e^7 2.18 e^8 ± 9.26 e^7	Kruskal Wallis: p=0.008; Chi^2=9.6 Pairwise Wilcox: LCP-FCP: p=0.05 LCP-HCP: p=0.008 FCP-HCP: p=1.0	Kruskal Wallis: p<0.0001; Chi^2=23.7 Pairwise Wilcox: org-min: p<0.0001 org-cryo: p=1.0 org-perm: p=0.015	
RCP2-54	organic mineral cryoturbated permafrost	3.19 e^5 ± 3.19 e^5 0.00 ± 0.00 - 0.00 ± 0.00	7.00 e^6 ± 2.40 e^6 7.81 e^5 ± 4.02 e^5 8.30 e^5 ± 7.02 e^5 0.00 ± 0.00	2.23 e^6 ± 7.31 e^5 2.61 e^6 ± 1.61 e^6 2.13 e^6 ± 1.40 e^6 4.32 e^5 ± 3.82 e^5	LCPs harbored 2.5 % of ddPCR-corr. reads assigned to this phylum.		
Sva0485	organic mineral cryoturbated permafrost	6.91 e^6 ± 2.49 e^6 1.84 e^5 ± 1.84 e^5 - 0.00 ± 0.00	0.00 ± 0.00 0.00 ± 0.00 0.00 ± 0.00 0.00 ± 0.00	0.00 ± 0.00 0.00 ± 0.00 0.00 ± 0.00 0.00 ± 0.00			LCP organic harbored 99.6 % of ddPCR-corr. reads assigned to this phylum
TA06	organic mineral cryoturbated permafrost	1.81 e^6 ± 5.15 e^5 3.68 e^5 ± 3.68 e^5 - 0.00 ± 0.00	0.00 ± 0.00 0.00 ± 0.00 0.00 ± 0.00 0.00 ± 0.00	0.00 ± 0.00 0.00 ± 0.00 0.00 ± 0.00 0.00 ± 0.00			LCP organic harbored 97 % of ddPCR-corr. reads assigned to this phylum
	organic mineral	7.58 e^6 ± 5.74 e^6 2.55 e^6 ± 1.99 e^6	1.45 e^6 ± 7.18 e^5 1.89 e^6 ± 1.02 e^6	4.23 e^5 ± 4.23 e^5 1.09 e^6 ± 4.20 e^5	Kruskal Wallis: p=0.131; Chi^2=4.1	Kruskal Wallis: p<0.0001; Chi^2=23.0	

Unknown Taxa on Phylum level	cryoturbated	-	$1.18\ e^7 \pm 3.97\ e^6$	$2.03\ e^6 \pm 7.93\ e^5$		The permafrost layer harbored 43 % of ddPCR-corr. reads assigned to this phylum.	
	permafrost	$4.17\ e^6 \pm 1.40\ e^6$	$1.46\ e^7 \pm 5.94\ e^6$	$4.90\ e^6 \pm 2.12\ e^6$			
Verrucomicrobiota	organic	$1.61\ e^8 \pm 4.78\ e^7$	$8.19\ e^8 \pm 1.35\ e^8$	$8.99\ e^8 \pm 1.15\ e^8$	Kruskal Wallis: p=0.0150; Chi^2=8.4 Pairwise Wilcox: LCP-FCP: p=0.035 LCP-HCP: p=0.027 FCP-HCP: p=1.0	Kruskal Wallis: p<0.0001; Chi^2=40.0 Pairwise Wilcox: org-min: p<0.0001 org-cryo:p=0.087 org-perm: p=<0.0001	
	mineral	$2.94\ e^7 \pm 5.19\ e^6$	$4.11\ e^7 \pm 1.07\ e^7$	$7.80e^7 \pm 2.48\ e^7$			
	cryoturbated	-	$2.35\ e^8 \pm 1.54\ e^8$	$1.91\ e^8 \pm 3.53\ e^7$			
	permafrost	$1.14\ e^7 \pm 5.77\ e^6$	$1.04\ e^8 \pm 4.74\ e^7$	$2.45\ e^7 \pm 1.10\ e^7$			
WPS-2	organic	$5.56\ e^5 \pm 4.10\ e^5$	$3.67\ e^6 \pm 1.80\ e^6$	$4.04\ e^6 \pm 2.36\ e^6$	LCPs harbored 6.4 % of ddPCR-corr. reads assigned to this phylum.		
	mineral	0.00 ± 0.00	$4.11\ e^5 \pm 2.52\ e^5$	0.00 ± 0.00			
	cryoturbated	-	$5.41\ e^5 \pm 5.41\ e^5$	$5.84\ e^5 \pm 3.89\ e^5$			
	permafrost	0.00 ± 0.00	0.00 ± 0.00	0.00 ± 0.00			

Presented are means ± SE (LCP_organic: n = 12, FCP_organic: n = 12, HCP_organic: n = 11, LCP_mineral: n = 2, FCP_mineral: n = 6, HCP_mineral: n = 6, FCP_cryoturbated: n = 5, HCP_cryoturbated: n = 6, LCP_permafrost: n = 6, FCP_permafrost: n = 7, HCP_permafrost: n = 6). Effects of polygon type, soil layer category, and their interaction were tested using linear mixed-effects models (Type III ANOVA), followed by Tukey-adjusted estimated marginal means for pairwise comparisons. When assumptions were not met, Kruskal–Wallis tests were performed, followed by Bonferroni-adjusted pairwise Wilcoxon tests for pairwise comparisons. For space saving reasons, the presented statistics refer mainly to the observations discussed in the main text. If phylum abundance estimates were too imbalanced for statistical testing, descriptive abundance information is stated instead. Abbreviations: HCPs = high-centered-, FCPs = flat-centered-, LCPs = low-centered polygons.

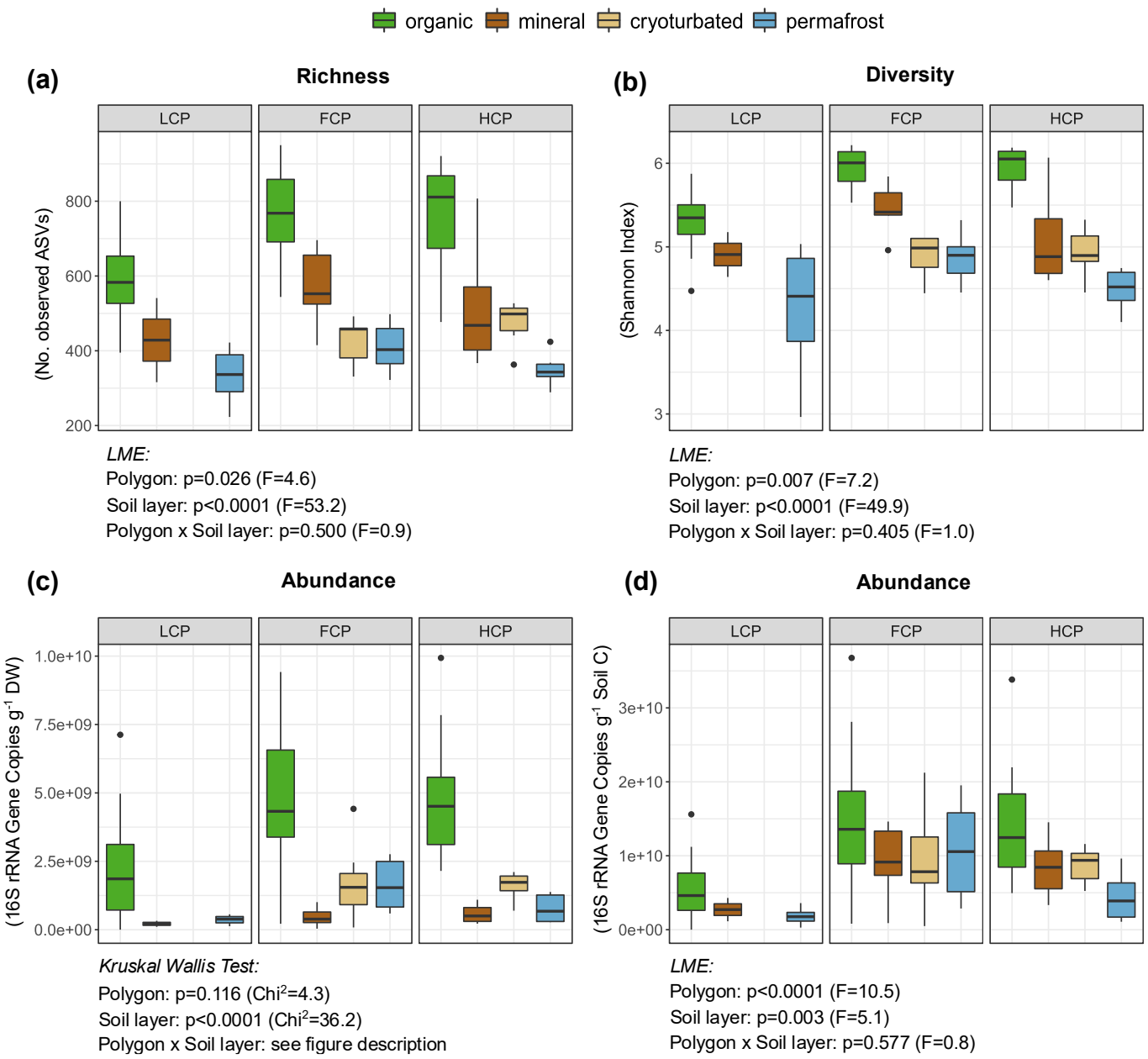

Figure S5. *Bacterial and archaeal richness, diversity, and abundance estimates across soil layers and ice-wedge polygon types. Panels show* ***(a)*** *richness (number of observed ASVs),* ***(b)*** *diversity (Shannon index),* ***(c)*** *abundance proxy (16S rRNA gene copies g⁻¹ DW soil), and* ***(d)*** *abundance normalized to soil carbon content (16S rRNA gene copies g⁻¹ soil C). Sample sizes: LCP_organic: n = 12, FCP_organic: n = 12, HCP_organic: n = 11; LCP_mineral: n = 2, FCP_mineral: n = 6, HCP_mineral: n = 6; FCP_cryoturbated: n = 7, HCP_cryoturbated: n = 6; LCP_permafrost: n = 6, FCP_permafrost: n = 7, HCP_permafrost: n = 6. Effects of polygon type and soil layer are indicated below the respective panels (linear mixed-effects models, ANOVA type III, or Kruskal Wallis tests). Pairwise comparisons were performed using Tukey-adjusted estimated marginal means or Bonferroni-adjusted pairwise Wilcoxon tests.*

Interactive effect: (c) Bacterial and archaeal abundance (16S rRNA gene copies g⁻¹ DW) *was lower in the organic layer of LCPs compared to FCPs and HCPs (Kruskal Wallis: p = 0.019, Chi² =*

7.92; pairwise Wilcoxon: LCP vs. FCP: p = 0.079, LCP vs. HCP: p = 0.032). In the permafrost layer, bacterial and archaeal abundance was also significantly lower in LCPs than FCPs (Kruskal Wallis p = 0.011, Chi² = 8.94; pairwise Wilcoxon: LCP vs. FCP: p = 0.010).

Bacterial and archaeal abundance (16S rRNA gene copies g^{-1} DW) varied across soil layers in all polygon types (Kruskal Wallis: LCP: p = 0.015, Chi² = 8.42; FCP: p = 0.001, Chi² = 15.59; HCP: p < 0.0001 Chi² = 23.07). In all polygon types, the organic layer harbored higher abundances than the permafrost layer (pairwise Wilcoxon: LCP: p = 0.039; FCP: p = 0.060; HCP: p = 0.007). In FCPs and HCPs, the organic layer additionally showed significantly higher abundances than the mineral layer (FCP: p = 0.026; HCP: p = 0.007). Abbreviations: HCPs = high-centered-, FCPs = flat-centered-, LCPs = low-centered polygons.

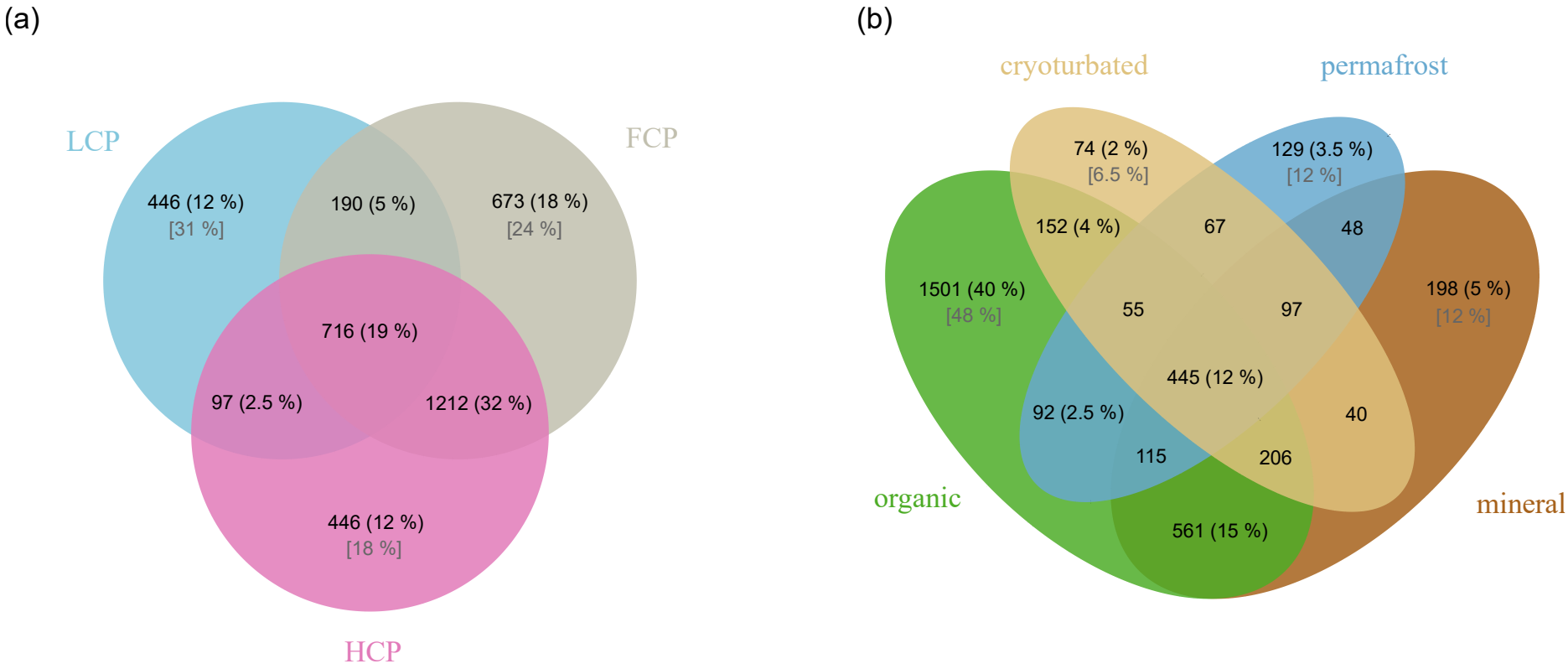

186

Figure S6. *Venn Diagram depicting the number of shared and unique bacterial and archaeal ASVs among* ***(a)*** *ice-wedge polygon types (low-centered polygon, LCP, n = 19; flat-centered polygon, FCP n = 30; high-centered polygon, HCP = 29) and* ***(b)*** *soil layers (organic topsoil = 35; mineral subsoil = 14; cryoturbated material = 11; permafrost = 19). Fractions of the shared and unique taxa relative to the total number of ASVs (n = 3780) are shown as percentages (%; black). The proportion of polygon-specific or soil layer-specific ASVs relative to the number of ASVs within each polygon type or soil layer are given in [%; grey].*

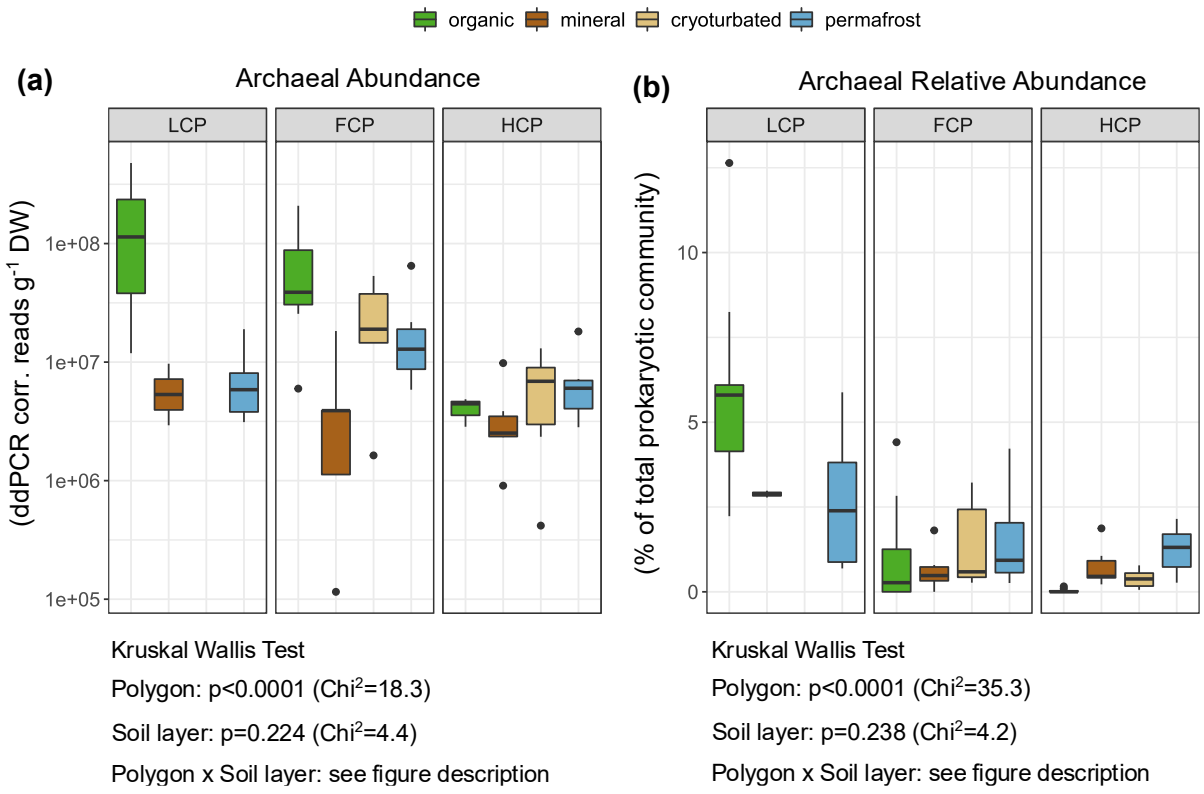

Figure S7. *Archaeal abundance across soil layers and ice-wedge polygon types. Panel* ***(a)*** *shows ddPCR-informed abundance estimates (gene copy number corrected reads* g^{-1} *DW). Panel* ***(b)*** *shows relative abundances (contribution of archaeal ddPCR-corrected reads to the total prokaryotic community, %). Sample sizes: LCP_organic: n = 12, FCP_organic: n = 12, HCP_organic: n = 11; LCP_mineral: n = 2, FCP_mineral: n = 6, HCP_mineral: n = 6; FCP_cryoturbated: n = 5, HCP_cryoturbated: n = 6; LCP_permafrost: n = 6, FCP_permafrost: n = 7, HCP_permafrost: n = 6. Archaeal abundance (a) is shown on a logarithmic scale for improved readability.*

Interactive effects: (a) Archaeal abundance (gene copy number–corrected reads g^{-1} ***DW)*** *was lower in HCP soils compared to LCP and FCP soils (HCP vs. LCP:* $p < 0.0001$*; HCP vs. FCP:* $p = 0.002$*). Within LCPs, archaeal abundance was notably higher in the organic layer than in the permafrost layer (*$p = 0.030$*), whereas no difference between layers were observed in FCPs. In HCPs, archaeal abundance in the organic layer was minimal and lower than in the cryoturbated (*$p = 0.030$*) and permafrost layers (*$p = 0.021$*).* ***(b) Archaeal relative abundance (%)*** *was higher in LCP soils compared to FCP and HCP soils (LCP vs. FCP:* $p < 0.0001$*; LCP vs. HCP:* $p < 0.0001$*), particularly in the organic layer (LCP vs. FCP:* $p = 0.0004$*; LCP vs. HCP:* $p = 0.0001$*). Within LCPs, relative abundance in the organic layer exceeded that in the permafrost layer (*$p = 0.039$*), whereas no differences were observed in FCPs. In HCPs, relative abundance in the organic layer was lower than in all other layers (organic vs. mineral:* $p = 0.003$*; organic vs. cryoturbated:* $p = 0.012$*; organic vs. permafrost:* $p = 0.003$*). Abbreviations: HCPs = high-centered-, FCPs = flat-centered-, LCPs = low-centered polygons.*

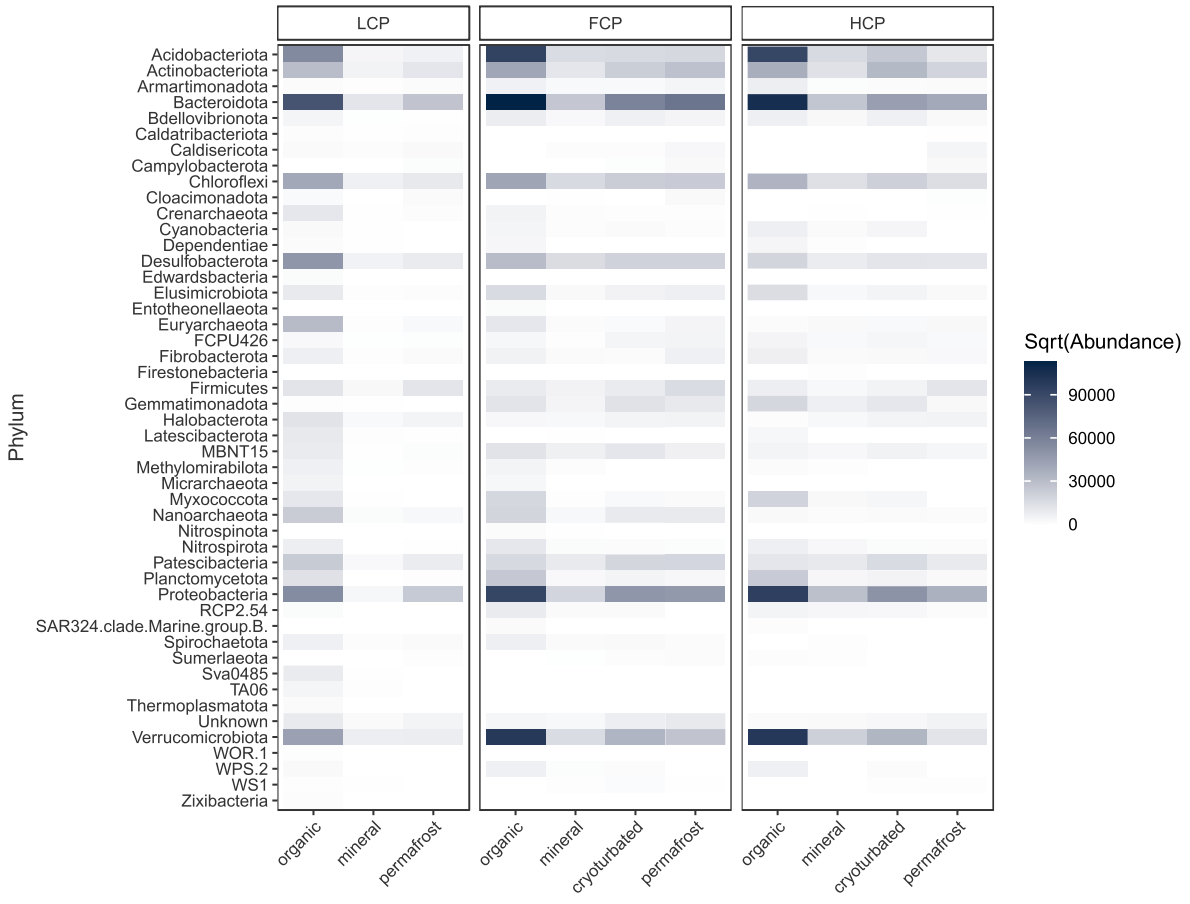

Figure S8. *Heatmap showing ddPCR-informed abundance estimates (gene copy number corrected reads g^{-1} DW soil) of bacterial and archaeal phyla across ice-wedge polygon types and soil layers (LCP_organic: n = 12, FCP_organic: n = 12, HCP_organic: n = 11, LCP_mineral: n = 2, FCP_mineral: n = 6, HCP_mineral: n = 6, FCP_cryoturbated: n = 7, HCP_cryoturbated: n = 6, LCP_permafrost: n = 6, FCP_permafrost: n = 7, HCP_permafrost: n = 6). Abundance estimates were square-root-transformed for improved visualization. "Unknown" denotes taxa that could not be assigned at the phylum level. Abbreviations: HCPs = high-centered-, FCPs = flat-centered-, LCPs = low-centered polygons.*

S4.2. Fungal communities

Table S7. *ddPCR-informed abundance estimates (gene copy number corrected reads g^{-1} DW soil) of fungal phyla across soil layers per polygon type.*

	Soil layer	LCP	FCP	HCP	Polygon effect	Soil layer effect	Interactive effect
Ascomycota	organic	$1.04\ e^7 \pm 3.18\ e^6$	$6.61\ e^7 \pm 2.18\ e^7$	$8.70\ e^7 \pm 2.44\ e^7$	Kruskal Wallis: p=0.361; Chi^2=2.0	Kruskal Wallis: p<0.0001; Chi^2=40.3 The organic layer harbored 96.7 % of ddPCR-corr. reads assigned to this phylum. org-min:p<0.0001 org-cryo:p<0.0004 org-perm:p<0.0001	Pairwise Wilcox organic: LCP-FCP: p=0.015 LCP-HCP: p=0.0004 FCP-HCP: p=0.844
	mineral	$3.45\ e^5 \pm 3.11\ e^5$	$7.37\ e^5 \pm 4.23\ e^5$	$1.63\ e^6 \pm 1.08\ e^6$			
	cryoturbated	-	$7.81\ e^5 \pm 3.61\ e^5$	$2.56\ e^6 \pm 5.03\ e^5$			
	permafrost	$6.18\ e^5 \pm 3.10\ e^5$	$4.07\ e^6 \pm 2.03\ e^6$	$3.34\ e^5 \pm 2.16\ e^5$			
Basidiomycota	organic	$3.32\ e^5 \pm 2.77\ e^5$	$2.00\ e^7 \pm 6.36\ e^6$	$3.16\ e^7 \pm 1.46\ e^7$	Kruskal Wallis: p=0.023; Chi^2=7.5 Pairwise Wilcox: LCP-FCP: p=0.049 LCP-HCP: p=0.055 FCP-HCP: p=1.0	Kruskal Wallis: p<0.0001; Chi^2=29.5 The organic layer harbored 99 % of ddPCR-corr. reads assigned to this phylum.	LCP organic harbored < 1% of ddPCR-corr. reads assigned to this phylum.
	mineral	$1.02\ e^3 \pm 1.02\ e^3$	$8.50\ e^4 \pm 5.86\ e^4$	$2.54\ e^5 \pm 2.39\ e^5$			
	cryoturbated	-	$3.68\ e^4 \pm 2.64\ e^4$	$4.78\ e^5 \pm 4.60\ e^5$			
	permafrost	$5.86\ e^3 \pm 4.65\ e^3$	$2.23\ e^4 \pm 1.02$ e4	$1.33\ e^4 \pm 1.21\ e^4$			
Chytridiomycota	organic	$3.97\ e^3 \pm 3.33\ e^3$	$1.35\ e^6 \pm 7.79\ e^5$	$5.27\ e^6 \pm 3.16\ e^6$	Kruskal Wallis: p=0.047; Chi^2=6.1 Pairwise Wilcox: LCP-FCP: p=0.047 LCP-HCP: p=0.087 FCP-HCP: p=1.0	Kruskal Wallis: p<0.0001; Chi^2=18.9 The organic layer harbored > 99 % of ddPCR-corr. reads assigned to this phylum.	LCP organic harbored < 1% of ddPCR-corr. reads assigned to this phylum.
	mineral	0.00 ± 0.00	$7.18\ e^2 \pm 4.80\ e^2$	$8.11\ e^2 \pm 7.07\ e^2$			
	cryoturbated	-	$2.18\ e^3 \pm 1.68\ e^3$	$2.16\ e^4 \pm 2.16\ e^4$			
	permafrost	0.00 ± 0.00	0.00 ± 0.00	0.00 ± 0.00			
Kickxellomycota	organic	$1.15\ e^4 \pm 1.10\ e^4$	$3.06\ e^5 \pm 2.53\ e^5$	$7.06\ e^3 \pm 7.06\ e^3$	Kruskal Wallis: p=0.898; Chi^2=0.2	The organic layer harbored 94 % of ddPCR-corr. reads assigned to this phylum.	LCP organic harbored < 5% of ddPCR-corr. reads assigned to this phylum.
	mineral	0.00 ± 0.00	0.00 ± 0.00	0.00 ± 0.00			
	cryoturbated	-	$6.77\ e^3 \pm 6.77\ e^3$	$3.37\ e^3 \pm 3.37\ e^3$			
	permafrost	0.00 ± 0.00	0.00 ± 0.00	$2.51\ e^3 \pm 2.51\ e^3$			

Mortierellomycota	organic	0.00 ± 0.00	4.25 e^4 ± 4.25 e^4	9.03 e^4 ± 5.51 e^4	Phylum is absent from LCP soils	The organic layer harbored 82 % of ddPCR-corr. reads assigned to this phylum.	
	mineral	0.00 ± 0.00	2.73 e^3 ± 2.73 e^3	3.67 e^2 ± 2.40 e^2			
	cryoturbated	-	3.14 e^3 ± 2.18 e^3	4.14 e^4 ± 4.14 e^4			
	permafrost	0.00 ± 0.00	4.58 e^3 ± 2.09 e^3	2.13 e^3 ± 2.13 e^3			
Rozellomycota	organic	0.00 ± 0.00	1.48 e^5 ± 1.03 e^5	2.30 e^3 ± 2.12 e^6	Phylum is absent from LCP soils.	The organic layer harbored 82 % of ddPCR-corr. reads assigned to this phylum.	LCP organic harbored >1 % of ddPCR-corr. reads assigned to this phylum.
	mineral	0.00 ± 0.00	0.00 ± 0.00	0.00 ± 0.00			
	cryoturbated	-	2.01 e^2 ± 2.01 e^2	0.00 ± 0.00			
	permafrost	0.00 ± 0.00	0.00 ± 0.00	0.00 ± 0.00			
Unknown Taxa on phylum level	organic	6.11 e^6 ± 3.39 e^6	9.61 e^7 ± 4.33 e^7	4.62 e^7 ± 1.39 e^7	Kruskal-Wallis: p=0.083; Chi^2=5.0	Kruskal Wallis: p<0.0001; Chi^2=31.7 The organic layer harbored > 92 % of ddPCR-corr. reads unassigned at phylum level	
	mineral	3.75 e4 ± 4.58 e^3	1.31 e^6 ± 6.52 e^5	1.34 e^6 ± 6.85 e^5			
	cryoturbated	-	6.52 e^6 ± 4.24 e^6	1.23 e^7 ± 7.57 e^6			
	permafrost	5.49 e^5 ± 5.25 e^5	2.12 e^6 ± 1.08 e^6	2.30 e^5 ± 1.13 e^5			
Zoopagomycota	organic	0.00 ± 0.00	0.00 ± 0.00	5.66 e^4 ± 5.66 e^4	Phylum is solely present in HCP organic.	Phylum is solely present in HCP organic.	HCP organic harbored 100% of ddPCR-corr. reads assigned to this phylum.
	mineral	0.00 ± 0.00	0.00 ± 0.00	0.00 ± 0.00			
	cryoturbated	-	0.00 ± 0.00	0.00 ± 0.00			
	permafrost	0.00 ± 0.00	0.00 ± 0.00	0.00 ± 0.00			

Presented are means ± SE (LCP_organic: n =12, FCP_organic: n = 12, HCP_organic: n = 11, LCP_mineral: n = 2, FCP_mineral: n = 6, HCP_mineral: n = 6, FCP_cryoturbated: n = 6, HCP_cryoturbated: n = 6, LCP_permafrost: n = 5, FCP_permafrost: n = 6, HCP_permafrost: n = 6, except for Basidiomycota where HCP_organic: n = 10). Effects of polygon type, soil layer category, and their interaction were tested using linear mixed-effects models (Type III ANOVA), followed by Tukey-adjusted estimated marginal means for pairwise comparisons. When assumptions were not met, Kruskal–Wallis tests were performed, followed by Bonferroni-adjusted pairwise Wilcoxon tests for pairwise comparisons. For space saving reasons, the presented statistics refer mainly to the observations discussed in the main text. If phylum abundance estimates were too imbalanced for statistical testing, descriptive abundance information is stated instead. Abbreviations: HCPs = high-centered-, FCPs = flat-centered-, LCPs = low-centered polygons.

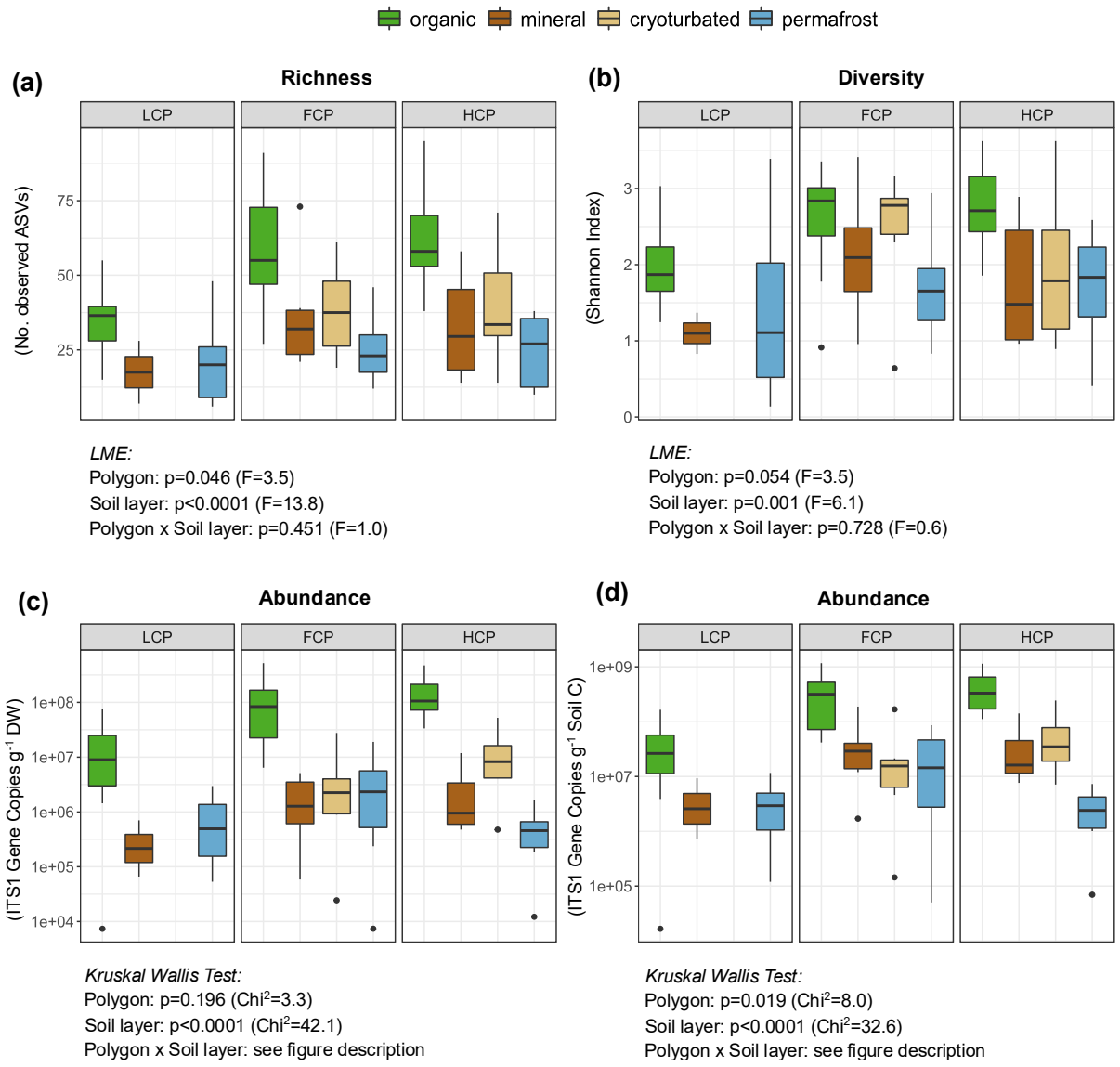

Figure S9. *Fungal richness, diversity, and abundance estimates across soil layers and ice-wedge polygon types. Panels show* ***(a)*** *richness (number of observed ASVs),* ***(b)*** *diversity (Shannon index),* ***(c)*** *abundance proxy (ITS gene copies g⁻¹ DW soil), and* ***(d)*** *abundance normalized to soil carbon content (ITS gene copies g⁻¹ soil C). Sample sizes: LCP_organic: n = 12, FCP_organic: n = 12, HCP_organic: n = 11, LCP_mineral: n = 2, FCP_mineral: n = 6, HCP_mineral: n = 6, FCP_cryoturbated: n = 6, HCP_cryoturbated: n = 6, LCP_permafrost: n = 5, FCP_permafrost: n = 6, HCP_permafrost: n = 6. Effects of polygon type and soil layer are indicated below the respective panels (linear mixed-effects models, ANOVA type III, or Kruskal Wallis tests). Pairwise comparisons were performed using Tukey-adjusted estimated marginal means or Bonferroni-adjusted pairwise Wilcoxon tests.*

Interactive effects: (c) Fungal abundance (ITS1 gene copies g⁻¹ DW) *was significantly lower in the organic layer of LCPs compared to FCPs and HCPs (Kruskal Wallis: p = 0.0004, Chi² = 15.91; pairwise Wilcoxon: LCP vs. FCP: p = 0.013, LCP vs. HCP: p = 0.0005). Fungal abundance varied across soil layers in all polygon types (Kruskal Wallis: LCP: p = 0.017, Chi² = 8.21; FCP: p = 0.0003, Chi² = 19.15; HCP: p < 0.0001, Chi² = 21.89). In all polygon types, the organic layer harbored higher fungal abundance*

than the permafrost layer (pairwise Wilcoxon: LCP: p = 0.039; FCP: p = 0.009; HCP: p = 0.007). In FCPs and HCPs, the organic layer also showed higher fungal abundance than in the mineral and cryoturbated layers (organic vs. mineral: FCP: p = 0.005; HCP: p = 0.007; organic vs. cryoturbated: FCP: p = 0.009; HCP: p = 0.013). ***(d) Fungal abundance normalized to soil carbon content (ITS1 gene copies g-1 soil C)*** *was higher in the organic layer than in the permafrost layer across all polygon types (pairwise Wilcoxon: LCP: p = 0.039; FCP: p = 0.021; HCP: p = 0.008). In FCPs and HCPs, it also exceeded abundances in the mineral and cryoturbated layers (organic vs. mineral: FCP: p = 0.026, HCP: p = 0.017; organic vs. cryoturbated: FCP: p = 0.012, HCP: p = 0.034). In HCPs, all layers exhibited higher fungal abundance per soil C than the permafrost layer (mineral vs. permafrost: p = 0.030; cryoturbated vs. permafrost: p = 0.049). Abbreviations: HCPs = high-centered-, FCPs = flat-centered-, LCPs = low-centered polygons.*

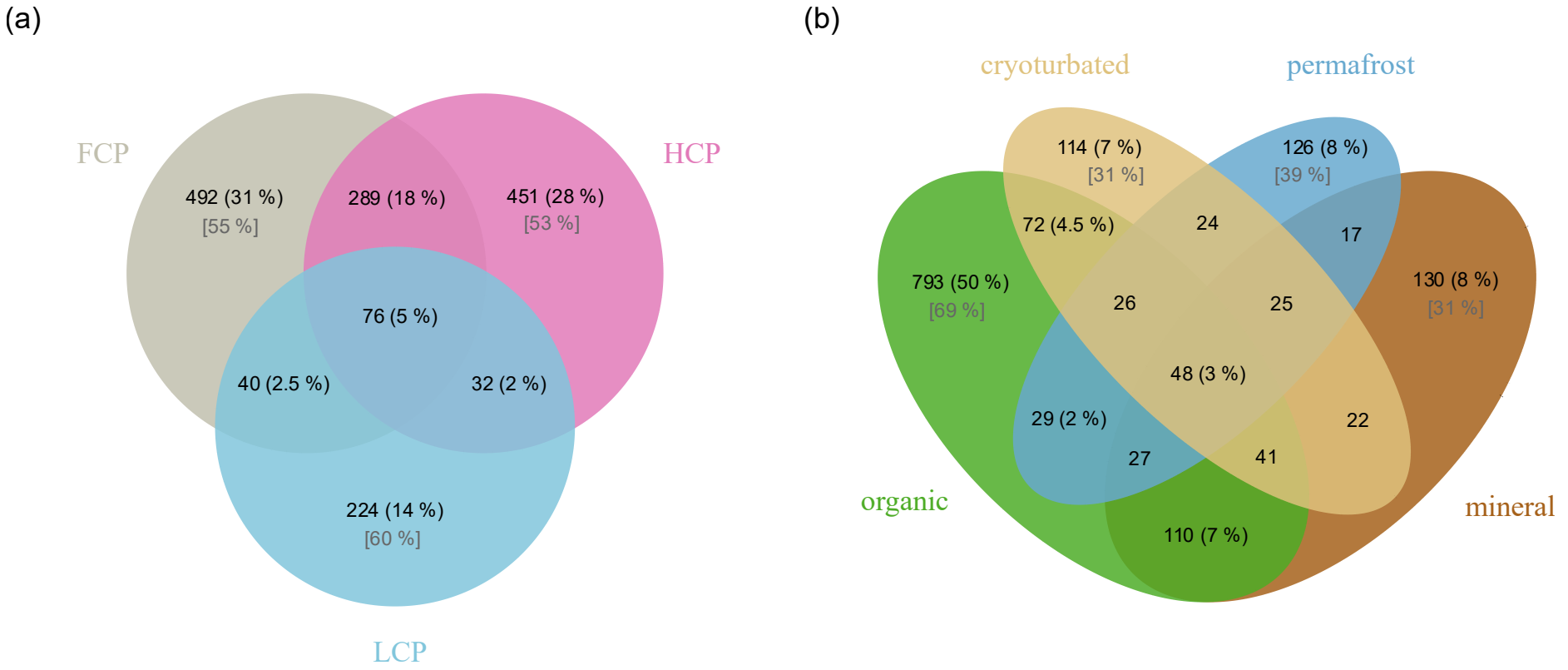

Figure S10. *Venn Diagram depicting the number of shared and unique fungal ASVs among* ***(a)*** *ice-wedge polygon types (low-centered polygon, LCP, n = 19; flat-centered polygon, FCP n = 30; high-centered polygon, HCP = 29) and among* ***(b)*** *soil layers (organic topsoil = 35, mineral subsoil = 14, cryoturbated material = 12, permafrost = 17). Fractions of the shared and unique taxa relative to the total number of ASVs (n = 1604) are shown as percentages (%; black). The proportion of polygon-specific or soil layer-specific ASVs relative to the number of ASVs within each polygon type or soil layer are given in [%; grey].*

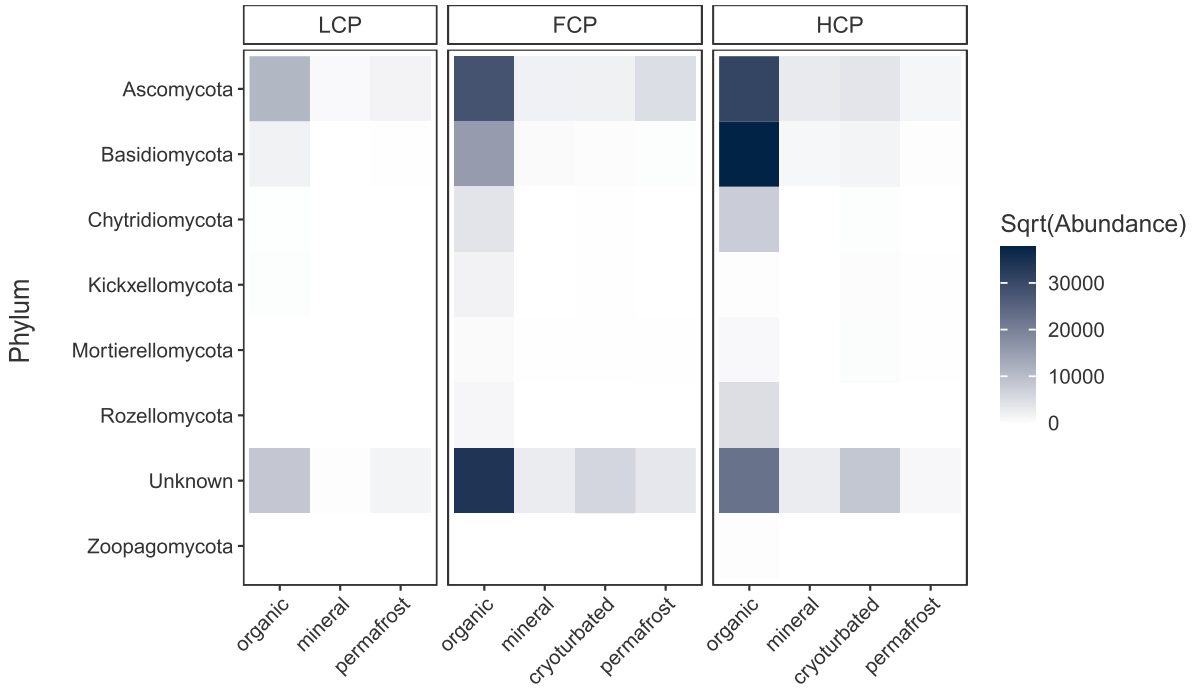

Figure S11. *Heatmap showing ddPCR-informed abundance estimates (gene copy number corrected reads* g^{-1} *DW soil) of fungal phyla across ice-wedge polygon types and soil layers (LCP_organic: n = 12, FCP_organic: n = 12, HCP_organic: n = 11, LCP_mineral: n = 2, FCP_mineral: n = 6, HCP_mineral: n = 6, FCP_cryoturbated: n = 6, HCP_cryoturbated: n = 6, LCP_permafrost: n = 5, FCP_permafrost: n = 6, HCP_permafrost: n=6). Abundance estimates were square-root-transformed for improved visualization. "Unknown" denotes taxa that could not be assigned at the phylum level. Abbreviations: HCPs = high-centered-, FCPs = flat-centered-, LCPs = low-centered polygons.*

S5. Extracellular enzymatic activity potential

We measured the potential activities of the six hydrolytic extracellular enzymes: β-D-1,4-cellobiosidase (exoglucanase), β-D-1,4-glucosidase, β-1,4-N-acetyl- glucosaminidase (exochitinase), leucine-aminopeptidase (protease), acid phosphatase, and sulfatase (Aryl-sulfate sulfohydrolase), using microplate fluorometric assays as described in Canarini et al., (2021). Per sample, one gram of soil was suspended in 100 ml sodium acetate buffer (100 mM, pH 5.5) and subsequently sonicated to an energy absorption of 350 J. 200 µl of the soil suspension and 50 µl of substrate were pipetted into black microtiter plates in five technical replicates. The used substrates were: 4-MUF-β-D-cellobioside, 4-MUF-β-D-glucoside, 4-MUF-N-acetyl-β-D-glucosaminide, L-Leucine-7-amino-4-methylcoumarin, 4-MUF-phosphate, 4-MUF-sulfate. 4-Methylumbelliferone (MUF) was used as standard for cellobiosidase, β-glucosidase, exochitinase, phosphatase and sulfatase, whereas 7-Amino-4-methylcoumarine (AMC) was used to calibrate protease activity. All plates were incubated at 20 °C for 15 minutes in the dark and fluorescence was measured at 365 nm excitation and 450 nm emission (Tecan Infinite M200fluorimeter, Werfen, Austria) every 30 minutes for 3 hours. Potential extracellular enzymatic activities were calculated considering the increase in fluorescence between measurement time points.

Table S8. *Correlations between potential extracellular enzymatic activities (nmol g^{-1} DW soil h^{-1}) and soil carbon, nitrogen, and phosphorus contents (mg g^{-1} DW soil).*

	Soil C	Soil N	Soil P
Betaglucosidase	ρ (79) = 0.743; **p < 0.0001**		
Exoglucanase	ρ (77) = 0.646 **p < 0.0001**		
Exochitinase	ρ (78) = 0.471 **p < 0.0001**	ρ (78) = 0.471 **p < 0.0001**	
Leucine-Aminopeptidase	ρ (79) = 0.663 **p < 0.0001**	ρ (79) = 0.660 **p < 0.0001**	
Acid Phosphatase	ρ (79) = 0.810 **p < 0.0001**		ρ (78) = 0.594 **p < 0.0001**
Sulfatase	ρ (75) = 0.680 **p < 0.0001**		

Presented are Spearman's rank-order correlation coefficients (ρ) with corresponding degrees of freedom (df) and two-sided p-values..

Table S9. *Interactive effects of polygon type and soil layer on potential extracellular enzymatic activities (nmol substrate g^{-1} soil C h^{-1}), corresponding to Figure 5.*

Soil Layer	Polygon	Betaglucosidase (emmeans)	Exoglucanase (pairwise Wilcox)	Exochitinase (emmeans)	Leucine Aminopeptidase (pairwise Wilcox)	Acid Phosphatase (pairwise Wilcox)
organic	LCP vs. FCP	**p<0.0001**; t=-6.6	**p=0.003**; w=15	**p=0.010**; t=-3.2	**p=0.070**; w=33	**p=0.000;** w=8
	LCP vs. HCP	**p=0.001**; t=-3.9	**p=0.002**; w=10	p=0.872; t=-0.5	**p=0.063**; w=28	p=0.118; w=32
	FCP vs. HCP	**p=0.035**; t=2.6	p=0.765; w=85	**p=0.034**; t=2.6	p=1.0; w=68	p=0.396; w=91
mineral	LCP vs. FCP	p=0.981; t=0.2	p=1.0; w=7	p=0.641; t=-0.9	p=0.729; w=2	p=1.0; w=5
	LCP vs. HCP	p=0.920; t=0.4	p=1.0; w=5	p=0.458; t=-1.2	p=1.0; w=3	p=1.0; w=6
	FCP vs. HCP	p=0.955; t=0.3	p=1.0; w=9	p=0.928; t=-0.4	p=1.0; w=20	p=1.0; w=18
cryoturbated	FCP vs. HCP	p=0.962; t=0.3	p=0.617; w=25	p=0.082; t=-2.2	p=0.830; w=23	p=0.170; w=11
permafrost	LCP vs. FCP	p=0.0895; t=-2.1	**p=0.010**; w=0	**p=0.026**; t=-2.7	p=0.115; w=6	p=1.0; w=18
	LCP vs. HCP	p=0.999; t=-0.1	p=0.197; w=6	**p=0.006**; t=-3.2	p=1.0; w=16	p=1.0; w=18
	FCP vs. HCP	p=0.100; t=2.1	**p=0.025**; w=40	p=0.814; t=-0.6	p=1.0; w=26	p=1.0; w=25

Polygon	Soil Layer	Betaglucosidase (emmeans)	Exoglucanase (pairwise Wilcox)	Exochitinase (emmeans)	Leucine Aminopeptidase (pairwise Wilcox)	Acid Phosphatase (pairwise Wilcox)
LCP	organic vs. mineral	p=0.870; t=0.8	p=1.0; w=15	p=0.874; t=0.8	p=0.171; w=20	p=0.235; w=20
	organic vs. permafrost	p=0.991; t=0.3	p=1.0; w=43	p=0.999; t=-0.1	p=0.110; w=59	p=0.147; w=52
	mineral vs. permafrost	p=0.949; t=-0.5	p=1.0; w=6	p=0.874; t=-0.8	p=1.0; w=6	p=0.877 w=5
FCP	organic vs. mineral	**p<0.0001**; t=6.9	**p=0.043**; w=56	**p=0.055**; t=2.6	p=0.882; w=52	**p=0.010;** w=70
	organic vs. cryoturbated	**p<0.0001**; t=5.1	p=0.23; w=67	p=0.904; t=0.7	p=0.708; w=61	**p=0.028;** w=76
	organic vs. permafrost	**p=0.006**; t=3.5	p=0.187; w=68	p=0.996; t=-0.2	**p=0.036**; w=75	**p=0.003;** w=84
	mineral vs. cryoturbated	p=0.991; t=-1.8	p=1.0; w=9	p=0.275; t=-1.8	p=1.0; w=16	p=1.0; w=17
	mineral vs. permafrost	**p=0.012**; t=-3.2	p=0.444; w=6	p=0.062; t=-2.6	p=1.0; w=30	p=1.0; w=23
	cryoturbated vs. permafrost	p=0.991; t=-1.5	p=1.0; w=18	p=0.848; t=-0.8	p=0.960; w=36	p=1.0; w=34
HCP	organic vs. mineral	**p<0.0001**; t=5.0	p=0.076; w=50	p=0.974; t=-0.4	p=0.472; w=51	p=0.109; w=57
	organic vs. cryoturbated	**p=0.020**; t=3.0	p=0.062; w=59	**p=0.0001**; t=-4.8	p=0.584; w=50	p=0.378; w=52
	organic vs. permafrost	**p=0.006**; t=3.4	**p=0.034**; w=61	**p=0.003**; t=-3.7	**p=0.013**; w=64	p=0.083; w=58
	mineral vs. cryoturbated	p=0.307; t=-1.8	p=1.0; w=12	**p=0.002**; t=-3.9	p=1.0; w=16	p=1.0; w=11
	mineral vs. permafrost	p=0.515; t=-1.4	p=1.0; w=13	**p=0.030**; t=-2.9	p=1.0; w=24	p=1.0; w=19
	cryoturbated vs. permafrost	p=0.983; t=0.4	p=1.0; w=20	p=0.756; t=1.0	p=0.394; w=30	p=0.272; w=31

Pairwise comparisons are shown (Tukey-adjusted estimated marginal means following linear mixed-effects models, or Bonferroni-adjusted pairwise Wilcoxon tests following Kruskal Wallis tests). No significant interaction was detected for sulfatase activity. Abbreviations: HCPs = high-centered-, FCPs = flat-centered-, LCPs = low-centered polygons.

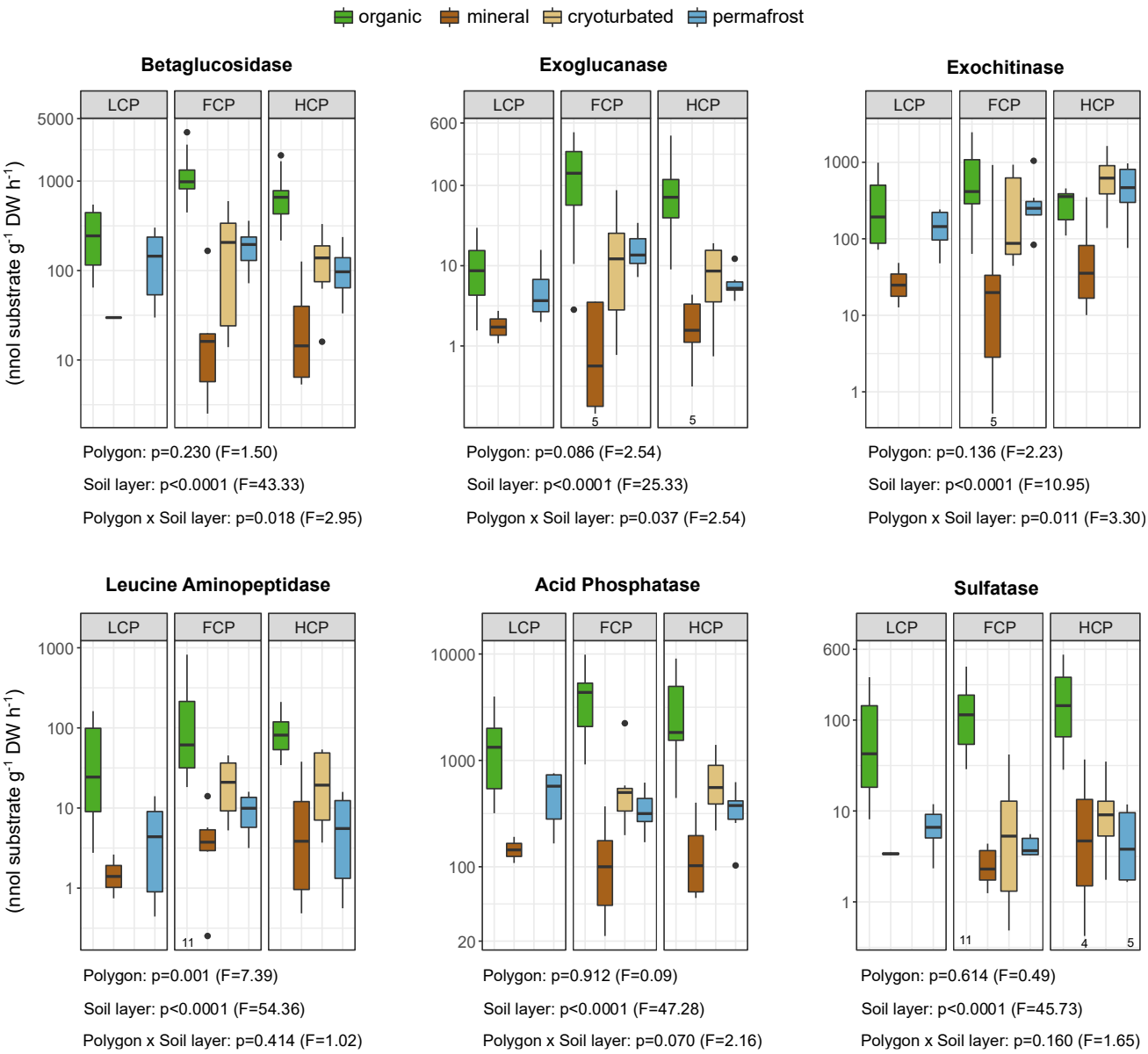

Figure S12. *Potential extracellular enzymatic activities across soil layers and ice-wedge polygon types. Potential activities of C-, N-, P- and S-acquiring enzymes are shown as rates (nmol substrate g $^{-1}$ DW soil h $^{-1}$) on a logarithmic scale for improved readability. Boxplots depict median values and interquartile ranges. Sample sizes: (LCP_organic: n = 12, FCP_organic: n = 12, HCP_organic: n = 11, LCP_mineral: n = 2, FCP_mineral: n = 6, HCP_mineral: n = 6, FCP_cryoturbated: n = 7, HCP_cryoturbated: n = 6, LCP_permafrost: n = 6, FCP_permafrost: n = 7, HCP_permafrost: n = 6. Individual deviations are indicated below the respective boxplots.*

Effects of polygon type and soil layer category are indicated below the respective panels (LME ANOVA type III or Kruskal Wallis test results). ***Interactive effects:*** *The organic layer of low-centered polygons (LCPs) exhibited lower betaglucosidase- (LCP vs. FCP: p < 0.0001, t = -5.1, LCP vs. HCP: p = 0.007, t = -3.2), exoglucanase- (LCP vs. FCP: p < 0.0001, t = -5.1, LCP vs. HCP: p = 0.0004, t = -4.2), and acid phosphatase- (LCP vs. FCP: p = 0.002, t = -3.6, LCP vs. HCP: p = 0.065, t = -2.3) -rates compared to the organic layers of*

flat-centered (FCPs) and high-centered polygons (HCPs). In addition, the permafrost layer of LCPs exhibited lower exochitinase activity than the permafrost samples of HCPs (LCP vs. HCP: p = 0.055, t = -2.4).

S6. Statistics

We employed linear-mixed-effects models (LMEs) to test all univariate variables for the fixed effects of 'ice-wedge polygon type' and 'soil layer category' plus their interaction. Therefore, we used the packages lme4 (Bates et al., 2015), lmerTest (Kuznetsova et al., 2017), emmeans,(Lenth et al., 2022) and car (Fox and Weisberg, 2019). While we acknowledge the difference in glaciation history between the examined sites, we anticipated only negligible historical influences on the characteristics of the recent SOM pool and microbial communities. Due to the sites' very similar landscape, climate, soils, and vegetation, we determined the random effect in the lme model as specific soil pit ID blocked within the sampling site (model<-lmer(variable~polygon.type*soil.layer + (1|site/soil pit)). Model results were inspected using the anova() function with the default being a type III analysis of variance (ANOVA). In the case of no interactive effect being observed we used type II ANOVA to account for potential effects of different treatment replicates (Langsrud, 2003) . We used the Estimated Marginal Means post hoc test to perform multiple comparisons on the fixed effects of polygon type and soil layer category (emmeans(model,pairwise~Polygon.type,adjust='tukey'),
ememans(model,pairwise~Soil.layer.,adjust='tukey'). In the case of an interactive effect being observed by ANOVA result and /or visual investigation of the data, we compared (a) differences between soil layers per type of polygon (emmeans(model,pairwise~Soil.layer. |Polygon.type, adjust='tukey') and (b) differences between polygon types per soil layer category (emmeans(model,pairwise~ Polygon.type |Soil.layer, adjust='tukey'). We checked for homogeneity of variances and normality of model residuals by inspecting frequency histograms, boxplots, QQ-plots, and via Shapiro and Levene tests. If model assumptions were not met, a log- or sqrt-transformation was applied. In case of no agreement with model assumptions after transformation, we conducted nonparametric tests (for variable specific details, see 10.5281/zenodo.18631833. Kruskal Wallis tests were used to test the effects of Polygon.type and Soil.layer, followed by pairwise two-sided Wilcoxon tests (function pairwise.wilcox.test(), p.adjust='bonferroni'). We also applied Wilcoxon tests on respectively subsetted parts of the dataset to check for possible interactive effects in a comparable manner as described for the LME models and additionally used faceted boxplots for checking the distribution of the examined parameter among all soil layer categories within each type of polygon.

We employed the phyloseq package (McMurdie and Holmes, 2013) for handling the multivariate datasets on amplicon sequencing and SOM chemical composition. Following Alteio et al., (2021), we applied a centered log-ratio (clr) data normalization (microbiome:: transform(phyloseq.object, "clr") and calculated Euclidean distance matrices (phyloseq::distance(phyloseq.object, "euclidean"). We performed Principal Component Analyses (PCAs) for visualization, employing the function 'phyloseq::ordinate()'. We used Permutational Multivariate Analysis of Variance (PERMANOVA) to explore the effects of polygon type and soil layer and their possible interaction (adonis()-function implemented in vegan with 999 permutations and p-adjust.m='bonferroni'; vegan version 2.5-7, Oksanen at al., 2020). We tested differences between polygon types and/or soil layer by pairwise multilevel comparisons (paiwise.adonis()-function implemented in vegan with 999 permutations and p.adjust.m='bonferroni)'. In case of interactive effects, we used subsetted datasets for making pairwise

245 tests. Analogously as described for the LME model, we tested for (a) differences between soil layers
246 within each polygon type and (b) for differences between polygon types for each soil layer. As
247 PERMANOVA test results are sensitive to heterogenous dispersions among the investigated groups,
248 we tested their variance of dispersion using Permutation Tests for Multivariate Dispersion Homogeneity
249 (PERMDIST), implemented in vegan (vegan::betadisper()-function) using 999 permutations and the
250 argument 'bias.adjust=T' for unequal sample numbers (Anderson, 2017). We used Venn diagrams
251 (get_vennlist(phyloseq.object) for visualizing the fraction of shared versus unique pyrolysis products
252 and/or microbial ASVs among polygon types and soil layers respectively (MicrobiotaProcess package,
253 (Xu et al., 2022)

S7. References:

Aitchison, J.: The statistical analysis of geochemical compositions, Journal of the International Association for Mathematical Geology, 16, 531–564, https://doi.org/10.1007/BF01029316, 1984.

Alteio, L. V., Séneca, J., Canarini, A., Angel, R., Jansa, J., Guseva, K., Kaiser, C., Richter, A., and Schmidt, H.: A critical perspective on interpreting amplicon sequencing data in soil ecological research, Soil Biology and Biochemistry, 160, https://doi.org/10.1016/j.soilbio.2021.108357, 2021.

Anderson, M.: Permutational Multivariate Analysis of Variance (PERMANOVA), 1–15, https://doi.org/10.1002/9781118445112.stat07841, 2017.

Apprill, A., McNally, S., Parsons, R., and Weber, L.: Minor revision to V4 region SSU rRNA 806R gene primer greatly increases detection of SAR11 bacterioplankton, Aquatic Microbial Ecology, 75, 129–137, 2015.

Barlow, J. T., Bogatyrev, S. R., and Ismagilov, R. F.: A quantitative sequencing framework for absolute abundance measurements of mucosal and lumenal microbial communities, Nat Commun, 11, 2590, https://doi.org/10.1038/s41467-020-16224-6, 2020.

Bates, D., Mächler, M., Bolker, B., and Walker, S.: Fitting Linear Mixed-Effects Models Using lme4, Journal of Statistical Software, 67, 1–48, https://doi.org/10.18637/jss.v067.i01, 2015.

Beck, H., Zimmermann, N., McVicar, T., Vergopolan, N., Berg, A., and Wood, E.: Present and future Köppen-Geiger climate classification maps at 1-km resolution, Scientific Data, 5, 180214, https://doi.org/10.1038/sdata.2018.214, 2018.

Brooks, G. R. and Lane, L. S.: A guide to the landscape of the Firth River Valley, Ivvavik National Park, 2011.

Buurman, P., Van Bergen, P. F., Jongmans, A. G., Meijer, E. L., Duran, B., and Van Lagen, B.: Spatial and temporal variation in podzol organic matter studied by pyrolysis-gas chromatography/mass spectrometry and micromorphology, European Journal of Soil Science, 56, 253–270, https://doi.org/10.1111/j.1365-2389.2004.00662.x, 2005.

Canarini, A., Schmidt, H., Fuchslueger, L., Martin, V., Herbold, C. W., Zezula, D., Gündler, P., Hasibeder, R., Jecmenica, M., Bahn, M., and Richter, A.: Ecological memory of recurrent drought modifies soil processes via changes in soil microbial community, Nature Communications, 12, 1–14, https://doi.org/10.1038/s41467-021-25675-4, 2021.

Couture, N. J. and Pollard, W. H.: A Model for Quantifying Ground-Ice Volume, Yukon Coast, Western Arctic Canada, Permafrost and Periglacial Processes, 28, 534–542, https://doi.org/10.1002/ppp.1952, 2017.

D'Angelo, E. and Crutchfield, J.: Rapid, Sensitive, Microscale Determination of Phosphate in Water and Soil, Journal of Environment Quality, 30, 2206, 2001.

Dyke, A. and Prest, V.: Late Wisconsinan and Holocene History of the Laurentide Ice Sheet, Géographie physique et Quaternaire, 41, 237–263, https://doi.org/10.7202/032681ar, 1987.

Fox, J. and Weisberg, S.: An R Companion to Applied Regression, Third Edition, Sage: Thousand Oaks, CA, USA, 2019.

Frank-Fahle, B. A., Yergeau, É., Greer, C. W., Lantuit, H., and Wagner, D.: Microbial functional potential and community composition in permafrost-affected soils of the NW Canadian Arctic, PLoS ONE, 9, https://doi.org/10.1371/journal.pone.0084761, 2014.

Fritz, M., Wetterich, S., Schirrmeister, L., Meyer, H., Lantuit, H., Preusser, F., and Pollard, W. H.: Eastern Beringia and beyond: Late Wisconsinan and Holocene landscape dynamics along the Yukon Coastal Plain, Canada, Palaeogeography, Palaeoclimatology, Palaeoecology, 319–320, 28–45, https://doi.org/10.1016/j.palaeo.2011.12.015, 2012.

Gloor, G. B., Macklaim, J. M., Pawlowsky-Glahn, V., and Egozcue, J. J.: Microbiome Datasets Are Compositional: And This Is Not Optional, Front. Microbiol., 8, 2224, https://doi.org/10.3389/fmicb.2017.02224, 2017.

González-Pérez, M., Buurman, P., Vidal-Torrado, P., and Martin-Neto, L.: Pyrolysis-Gas Chromatography/Mass Spectrometry Characterization of Humic Acids in Coastal Spodosols from Southeastern Brazil, Soil Science Society of America Journal, 76, 961–971, https://doi.org/10.2136/sssaj2011.0178, 2012.

Canadian Climate Normals & Averages: http://climate.weather.gc.ca/climate_normals/index_e.html.

Hempfling, R. and Schulten, H. R.: Chemical characterization of the organic matter in forest soils by Curie point pyrolysis-GC/MS and pyrolysis-field ionization mass spectrometry, Organic Geochemistry, 15, 131–145, https://doi.org/10.1016/0146-6380(90)90078-E, 1990.

Kim, S., Chen, J., Cheng, T., Gindulyte, A., He, J., He, S., Li, Q., Shoemaker, B. A., Thiessen, P. A., Yu, B., Zaslavsky, L., Zhang, J., and Bolton, E. E.: PubChem 2023 update., Nucleic acids research, 51, D1373–D1380, https://doi.org/10.1093/nar/gkac956, 2023.

Kuo, S.: Phosphorus. In Methods of Soil Analysis, Part 3: Chemical Methods., Soil Science Society of America, 869–919 pp., 1996.

Kuznetsova, A., Brockhoff, P. B., and Christensen, R. H. B.: lmerTest Package: Tests in Linear Mixed Effects Models, Journal of Statistical Software, 82, 1–26, https://doi.org/10.18637/jss.v082.i13, 2017.

Langsrud, Ø.: ANOVA for unbalanced data: Use Type II instead of Type III sums of squares, Statistics and computing, 13, 163–167, 2003.

Lenth, R. V., Buerkner, P., Herve, M., Love, J., Miguez, F., Riebl, H., and Singmann, H.: Package "Emmeans"(Version R Package 1.7. 2): Estimated Marginal Means, Aka Least-Squares Means [Computer Software], 2022.

Martin, V., Schmidt, H., Canarini, A., Koranda, M., Hausmann, B., Müller, C. W., and Richter, A.: Soil cover shapes organic matter pools and microbial communities in soils of maritime Antarctica, Geoderma, 446, 116894, https://doi.org/10.1016/j.geoderma.2024.116894, 2024.

McMurdie, P. J. and Holmes, S.: phyloseq: An R Package for Reproducible Interactive Analysis and Graphics of Microbiome Census Data, PLOS ONE, 8, 1–11, https://doi.org/10.1371/journal.pone.0061217, 2013.

Ninnes, S., Tolu, J., Meyer-Jacob, C., Mighall, T. M., and Bindler, R.: Investigating molecular changes in organic matter composition in two Holocene lake-sediment records from central Sweden using pyrolysis-GC/MS, Journal of Geophysical Research: Biogeosciences, 122, 1423–1438, https://doi.org/10.1002/2016JG003715, 2017.

Oksanen, J., Blanchet, F. G., Friendly, M., Kindt, R., Legendre, P., McGlinn, D., Minchin, P. R., O'Hara, R. B., Simpson, G. L., Solymos, P., Stevens, M. H. H., Szoecs, E., Wagner, H., 2020. vegan: Community Ecology Package. R package version 2.5-7. https://CRAN.R-project.org/package=vegan.

Parada, A. E., Needham, D. M., and Fuhrman, J. A.: Every base matters: assessing small subunit rRNA primers for marine microbiomes with mock communities, time series and global field samples, Environmental Microbiology, 18, 1403–1414, https://doi.org/10.1111/1462-2920.13023, 2016.

Pjevac, P., Hausmann, B., Schwarz, J., Kohl, G., Herbold, C. W., Loy, A., and Berry, D.: An Economical and Flexible Dual Barcoding, Two-Step PCR Approach for Highly Multiplexed Amplicon Sequencing, Frontiers in Microbiology, 12, https://doi.org/10.3389/fmicb.2021.669776, 2021.

Põlme, S., Abarenkov, K., Henrik Nilsson, R., Lindahl, B. D., Clemmensen, K. E., Kauserud, H., Nguyen, N., Kjøller, R., Bates, S. T., Baldrian, P., Frøslev, T. G., Adojaan, K., Vizzini, A., Suija, A., Pfister, D., Baral, H. O., Järv, H., Madrid, H., Nordén, J., Liu, J. K., Pawlowska, J., Põldmaa, K., Pärtel, K., Runnel, K., Hansen, K., Larsson, K. H., Hyde, K. D., Sandoval-Denis, M., Smith, M. E., Toome-Heller, M., Wijayawardene, N. N., Menolli, N., Reynolds, N. K., Drenkhan, R., Maharachchikumbura, S. S. N., Gibertoni, T. B., Læssøe, T., Davis, W., Tokarev, Y., Corrales, A., Soares, A. M., Agan, A., Machado, A. R., Argüelles-Moyao, A., Detheridge, A., de Meiras-Ottoni, A., Verbeken, A., Dutta, A. K., Cui, B. K., Pradeep, C. K., Marín, C., Stanton, D., Gohar, D., Wanasinghe, D. N., Otsing, E., Aslani, F., Griffith, G. W., Lumbsch, T. H., Grossart, H. P., Masigol, H., Timling, I., Hiiesalu, I., Oja, J., Kupagme, J. Y., Geml, J., Alvarez-Manjarrez, J., Ilves, K., Loit, K., Adamson, K., Nara, K., Küngas, K., Rojas-Jimenez, K., Bitenieks, K., Irinyi, L., Nagy, L. L., Soonvald, L., Zhou, L. W., Wagner, L., Aime, M. C., Öpik, M., Mujica, M. I., Metsoja, M., Ryberg, M., Vasar, M., Murata, M., Nelsen, M. P., Cleary, M., Samarakoon, M. C., Doilom, M., Bahram, M., Hagh-Doust, N., Dulya, O., Johnston, P., Kohout, P., Chen, Q., Tian, Q., Nandi, R., Amiri, R., Perera, R. H., et al.: FungalTraits: a user-friendly traits database of fungi and fungus-like stramenopiles, Fungal Diversity, 105, https://doi.org/10.1007/s13225-020-00466-2, 2020.

Rampton, V. N.: Quaternary Geology Yukon Coastal Plain, Yukon Territory-Northwest Territory, , https://doi.org/10.4095/111348, 1982.

Said, M., John, G., Mhilu, C., and Manyele, S.: The Study of Kinetic Properties and Analytical Pyrolysis of Coconut Shells, Journal of Renewable Energy, 2015, 307329, https://doi.org/10.1155/2015/307329, 2015.

Saiz-Jimenez, C. and De Leeuw, J. W.: Chemical characterization of soil organic matter fractions by analytical pyrolysis-gas chromatography-mass spectrometry, Journal of Analytical and Applied Pyrolysis, 9, 99–119, https://doi.org/10.1016/0165-2370(86)85002-1, 1986.

Schulten, H. R. and Schnitzer, M.: The chemistry of soil organic nitrogen: A review, Biology and Fertility of Soils, 26, 1–15, https://doi.org/10.1007/s003740050335, 1997.

Shen, Q., Suarez-Abelenda, M., Camps-Arbestain, M., Calvelo Pereira, R., McNally, S. R., and Kelliher, F.: Data on the organic matter characteristics of New Zealand soils under different land uses, Data in Brief, 21, 620–638, https://doi.org/10.1016/j.dib.2018.10.016, 2018.

Smith, D. P. and Peay, K. G.: Sequence depth, not PCR replication, improves ecological inference from next generation DNA sequencing., PloS one, 9, e90234, https://doi.org/10.1371/journal.pone.0090234, 2014.

Soil Classification Working Group: The Canadian System of Soil Classification, 187 pp. pp., 1998.

Speetjens, N. J., Tanski, G., Martin, V., Wagner, J., Richter, A., Hugelius, G., Boucher, C., Lodi, R., Knoblauch, C., Koch, B. P., Wünsch, U., Lantuit, H., and Vonk, J. E.: Dissolved organic matter characterization in soils and streams in a small coastal low-Arctic catchment, Biogeosciences, 19, 3073–3097, https://doi.org/10.5194/bg-19-3073-2022, 2022.

Stewart, C. E.: Evaluation of angiosperm and fern contributions to soil organic matter using two methods of pyrolysis-gas chromatography-mass spectrometry, Plant and Soil, 351, 31–46, https://doi.org/10.1007/s11104-011-0927-3, 2012.

Tarnocai, C.: Northern Soil Research in Canada - Cryosols: Permafrost-Affected Soils, edited by: Kimble, J. M., Springer Berlin Heidelberg, Berlin, Heidelberg, 29–43, https://doi.org/10.1007/978-3-662-06429-0_3, 2004.

Tolu, J., Gerber, L., Boily, J.-F., and Bindler, R.: High-throughput characterization of sediment organic matter by pyrolysis–gas chromatography/mass spectrometry and multivariate curve resolution: A

promising analytical tool in (paleo)limnology, Analytica Chimica Acta, 880, 93–102, https://doi.org/10.1016/j.aca.2015.03.043, 2015.

Vancampenhout, K., Wouters, K., De Vos, B., Buurman, P., Swennen, R., and Deckers, J.: Differences in chemical composition of soil organic matter in natural ecosystems from different climatic regions - A pyrolysis-GC/MS study, Soil Biology and Biochemistry, 41, 568–579, https://doi.org/10.1016/j.soilbio.2008.12.023, 2009.

Wagner, J., Martin, V., Speetjens, N. J., A'Campo, W., Durstewitz, L., Lodi, R., Fritz, M., Tanski, G., Vonk, J. E., Richter, A., Bartsch, A., Lantuit, H., and Hugelius, G.: High resolution mapping shows differences in soil carbon and nitrogen stocks in areas of varying landscape history in Canadian lowland tundra, Geoderma, 438, 116652, https://doi.org/10.1016/j.geoderma.2023.116652, 2023.

Walker, D. A., Raynolds, M. K., Daniëls, F. J. A., Einarsson, E., Elvebakk, A., Gould, W. A., Katenin, A. E., Kholod, S. S., Markon, C. J., Melnikov, E. S., Moskalenko, N. G., Talbot, S. S., Yurtsev, B. A. (†), and Team, T. other members of the C.: The Circumpolar Arctic vegetation map, Journal of Vegetation Science, 16, 267–282, https://doi.org/10.1111/j.1654-1103.2005.tb02365.x, 2005.

Westerveld, L., Kurvits, T., Schoolmeester, T., Eckhoff, T., Overduin, P., Fritz, M., Alfthan, B., Sinisalo, A., and Mulelid, O.: Arctic Permafrost Atlas, https://doi.org/10.61523/KPJI4549, 2023.

White, Bruns, T., Lee, S., and Taylor, J.: White, T. J., T. D. Bruns, S. B. Lee, and J. W. Taylor. Amplification and direct sequencing of fungal ribosomal RNA Genes for phylogenetics, 315–322, 1990.

Xu, S., Li, Z., Tang, W., Dai, Z., Zhou, L., Feng, T., Chen, M., Liu, S., Fu, X., Wu, T., Hu, E., and Yu, G.: MicrobiotaProcess: A comprehensive R package for managing and analyzing microbiome and other ecological data within the tidy framework, , https://doi.org/10.21203/rs.3.rs-1284357/v1, 2022.